Ocean Engineering 129 (2017) 133–148

Contents lists available at ScienceDirect

Ocean Engineering

journal homepage: www.elsevier.com/locate/oceaneng

Verification and Validation exercises for the flow around the KVLCC2 tanker at model and full-scale Reynolds numbers

F.S. Pereira[a,b,*], L. Eça[b], G. Vaz[c]

[a] Maritime Research Institute Netherlands Academy, 2 Haagsteeg, 6708 PM Wageningen, The Netherlands
[b] Instituto Superior Técnico, Av. Rovisco Pais 1, 1049-001 Lisbon, Portugal
[c] Maritime Research Institute Netherlands, 2 Haagsteeg, 6708 PM Wageningen, The Netherlands

ARTICLE INFO

Keywords:
Modelling error
Numerical error
Turbulence modelling
RANS
KVLCC2

ABSTRACT

This paper presents the quantification of numerical and modelling errors for the solution of the flow around the KVLCC2 tanker at model-scale Reynolds number. Numerical errors are also quantified for full-scale Reynolds number simulations to address the numerical accuracy of the prediction of scale-effects. The calculations are performed with the solver ReFRESCO using fourteen distinct Reynolds-Averaged Navier-Stokes (RANS) equations models. The quantities of interest for the Validation exercises at model-scale are the resistance coefficient and the velocity and turbulence kinetic energy fields at the propeller plane. Modelling errors are estimated using the ASME V&V20 procedure which requires numerical and experimental data with their respective uncertainties. Numerical uncertainties are dominated by the contribution of the discretization error, which is determined by grid refinement studies. Scale-effects are also assessed for the wake-fraction and form-factor. The outcome shows that quantifying modelling errors is not a trivial exercise that depends on the quality and details of simulations and experiments. Nonetheless, it is also evident that a quantitative evaluation of modelling errors is more reliable than traditional graphical comparisons of simulations and experiments. Full-scale results show scale-effects larger than numerical uncertainties that are illustrated for the form-factor and wake-fraction.

1. Introduction

Computational Fluid Dynamics (CFD) has become an integral part of the design process of many engineering applications including ship hydrodynamics. Its ability to give detailed information of the flow field at a much faster turnaround time and cheaper cost than Experimental Fluid Dynamics (EFD) made CFD a valuable complement to the traditional model testing. Nonetheless, as for EFD, the credibility of CFD simulations requires the assessment of the modelling (facility quality in EFD) and numerical (measuring instruments quality in EFD) uncertainties to avoid the risk of taking erroneous conclusions.

Flows around ships are governed by mass and momentum conservation that are expressed in the incompressible continuity and Navier-Stokes equations. However, ship flows occur at high Reynolds numbers which means turbulent flows exhibiting a wide range of spatial and temporal scales. In such conditions, the direct solution of the Navier-Stokes is not feasible and so alternative mathematical models must be applied in practice.

Nowadays, Scale-Resolving Simulation (SRS) models, as for example Spalart et al. (1997) or Girimaji (2005), are able to solve directly part of the turbulence field, reducing the extra modelling to the smallest scales that tend to be easier to model (isotropic). However, its application to wall bounded flows is substantially more demanding than the Reynolds-Averaged Navier-Stokes (RANS) equations, which are still the most common mathematical model for engineering applications (Larsson et al., 2013; National Maritime Research Institute, 2015). Furthermore, for ships with no drift angle, time-averaged RANS should be able to accurately predict the mean flow field and force coefficients. However, the modelling accuracy of RANS is strongly dependent on the selected turbulence model that provides the values of the Reynolds stresses produced by the averaging process. Therefore, the turbulence model is the main source of modelling errors

Abbreviations: ASME, American Society of Mechanical Engineers; BSL, Baseline; CFD, Computational Fluid Dynamics; DES, Detached-Eddy Simulation; EARSM, Explicit Algebraic Reynolds-Stresses Model; EFD, Experimental Fluid Dynamics; ITTC, International Towing Tank Conference; KRISO, Korea Research Institute of Ships and Ocean; KVLCC2, KRISO Very Large Crude Carrier 2; LES, Large-Eddy Simulation; MARIN, Maritime Research Institute Netherlands; RANS, Reynolds-Averaged Navier-Stokes equations; ReFRESCO, Reliable and Fast RANS Equations solver for Ships and Construction Offshore; SRS, Scale-Resolving Simulation; SST, Shear-Stress Transport; TNT, Turbulent Non-Turbulent

* Corresponding author at: Instituto Superior Técnico, Av. Rovisco Pais 1, 1049-001 Lisbon, Portugal.
E-mail addresses: filipemsoares@ist.utl.pt (F.S. Pereira), luis.eca@ist.utl.pt (L. Eça), g.vaz@marin.nl (G. Vaz).

http://dx.doi.org/10.1016/j.oceaneng.2016.11.005
Received 3 August 2016; Received in revised form 1 October 2016; Accepted 12 November 2016
Available online 23 November 2016

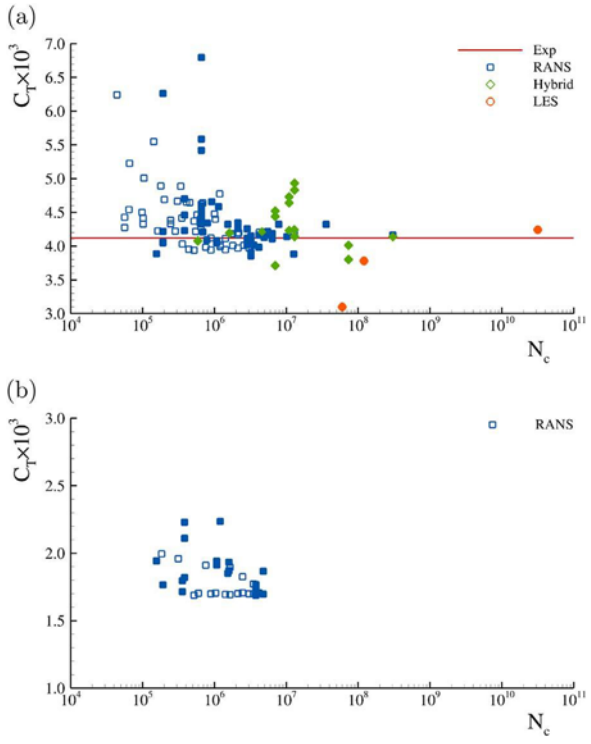

Fig. 1. Results available in the open scientific literature (Abdel-Maksoud et al., 2000; Beddhu et al., 2000; Chou et al., 2000; Deng and Visonneau, 2000; Hoekstra et al., 2000; Kim, 2000; Kim and Van, 2000; Rhee and Hino, 2000; Svennberg, 2000; Guo and Steen, 2010; Kim et al., 2010; Martio et al., 2010; Schneider, 2010; Xing et al., 2010; Yu et al., 2010; VIRTUE – The Virtual Tank Utility in Europe, 2007a, 2007b; Toxopeus, 2011; Nishikawa et al., 2012, 2013; Abbas et al., 2013; Toxopeus et al., 2014) for the viscous resistance coefficient C_T at model (4.60×10^6) and full-scale (2.03×10^9) Reynolds numbers as a function of the number of grid cells N_c and mathematical model: RANS, Hybrid and LES. Filled symbols represent the best solution obtained in each reference (finest spatial resolution or highest-order convection scheme). Experimental measurement taken from Kim et al. (2001) (estimated experimental uncertainty is 1%). (a) Model-scale. (b) Full-scale.

in the solution of the RANS equations for the type of flows addressed in this work.

On the other hand, simulation of ship flows based on the RANS equations requires numerical solutions, which are affected by discretization, iterative and round-off errors (Roache, 1998, 2009; Oberkampf and Roy, 2010; The American Society of Mechanical Engineers, 2009). Therefore, numerical uncertainties must be assessed to properly quantify modelling errors (Roache, 1998, 2009; Oberkampf and Roy, 2010; The American Society of Mechanical Engineers, 2009).

In order to illustrate the relevance of modelling and numerical errors on ship hydrodynamics simulations, a numerical literature review has been performed for a representative and widely studied crude tanker: the KRISO Very Large Crude Carrier 2 (KVLCC2). Fig. 1 depicts the resistance coefficient C_T from 160 results published in the open literature for model (4.60×10^6) and full-scale (2.03×10^9) Reynolds numbers. The data is presented as a function of the mathematical model and number of grid cells. Three groups of mathematical models are considered: RANS with several turbulence models ($k-\omega$, $k-\epsilon$, ...), Hybrid models (Detached Eddy Simulation, DES) and Large-Eddy Simulation (LES). In the plot, no distinction is made between domain sizes, grid topologies, turbulence models and boundary conditions, i.e. free surface effects[1] and the use of wall functions (common at full-scale Reynolds numbers). The results are collected from the Gothenburg workshops of Abdel-Maksoud et al. (2000), Beddhu et al. (2000), Chou et al. (2000), Deng and Visonneau (2000), Hoekstra et al. (2000), Kim (2000), Kim and Van (2000), Rhee and Hino (2000), Svennberg (2000) and Guo and Steen (2010), Kim et al. (2010), Martio et al. (2010), Schneider (2010), Xing et al. (2010), Yu et al. (2010), the EU cooperative project Virtue workshops of VIRTUE – The Virtual Tank Utility in Europe (2007a), VIRTUE – The Virtual Tank Utility in Europe (2007b) and some additional studies (Toxopeus, 2011; Nishikawa et al., 2012, 2013; Abbas et al., 2013; Toxopeus et al., 2014). The largest dispersion of C_T values at model-scale is observed for grids with less than one million cells, which suggests a significant influence of discretization errors. For such range of grid resolutions the difference between experiments and simulations (comparison error E_{C_T}) may reach 70%. For grids with more than two million cells[2] the average E_{C_T} obtained from RANS simulations is −0.6% of the experimental value, but the standard deviation is 3.7%, which is more than the desirable 1% accuracy in the prediction of C_T. On the other hand, Hybrid models results do not show any improvement in the standard deviation of E_{C_T}, which is 9% for grids with more than two million cells and the range of values obtained for the three LES solutions exhibits a difference in the predicted C_T of 28%. A similar dispersion of data is also observed in the full-scale results that are depicted in Fig. 1b. This scenario raises a legitimate question: is this spread of data a consequence of modelling errors (turbulence models) or numerical errors (or both)?

The only way to answer this question is to apply available procedures (The American Society of Mechanical Engineers, 2009, 2016) to estimate the modelling error, which require the knowledge of the experimental and numerical uncertainties. To this end, this work presents the quantification of numerical and modelling errors for the flow around the same KVLCC2 tanker at model-scale Reynolds number, i.e. Solution Verification and Validation exercises. On the other hand, numerical errors are quantified for full-scale simulations to address the numerical accuracy of the prediction of scale-effects. Numerical uncertainties are estimated for all flow conditions using grid refinement studies (Eça and Hoekstra, 2014), whereas modelling errors are quantified for the model-scale simulations using the ASME V&V20 procedures (The American Society of Mechanical Engineers, 2009, 2016) and the experimental data of Kim et al. (2001) and Lee et al. (2003). The calculations are carried out with the solver ReFRESCO (ReFRESCO, 2016) using fourteen distinct RANS turbulence models:

- Spalart and Allmaras (1992);
- Menter (1997);
- $\sqrt{k}L$ Menter et al. (2006);
- Low-Reynolds $k-\epsilon$ Abe et al. (1994);
- $k-\omega$ Wilcox (1988) and Wilcox (1998) versions;
- $k-\omega$ Turbulent Non-Turbulent (TNT) Kok (2000);
- $k-\omega$ BaSeLine (BSL) Menter (1994);
- $k-\omega$ Shear-Stress Transport (SST) Menter (1994, 2003) versions;
- $k-\sqrt{k}L$ Menter et al. (2006);
- $k-\omega$ BSL Explicit Algebraic Reynolds-Stresses Model (EARSM) Hellsten (2005) (two versions).
- $k-\omega$ TNT EARSM Dol et al. (2002).

The first eleven models are isotropic eddy-viscosity models, while the last three models consider the anisotropy of the Reynolds stresses. Although there are some reviews and studies addressing the role of turbulence modelling and numerical errors for the present test-case (see for instance Larsson et al., 2013; Toxopeus et al., 2013; Guo et al., 2013), the present work compares the former fourteen models under

[1] It must be mentioned that most of the data correspond to simulations neglecting free-surface effects.

[2] Using only the best results of each reference, the average E_{C_T} obtained from RANS simulations is 0.01% and the standard deviation is 3.2%

the same conditions: computational domain, grids, boundary conditions, discretization techniques, etc. Naturally, we could have restricted the number of turbulence models selected. However, one of the goals of this exercise is to check the effect of the turbulence model on the numerical robustness, i.e. on the ability to reduce the iterative error to negligible levels. Furthermore, it is also important to investigate the influence of the turbulence models on the convergence properties of the discretization error of the selected flow quantities, which are the resistance coefficient and the velocity and turbulence kinetic energy fields at the propeller plane. Nonetheless, for the simulations at full-scale Reynolds number only four models are used: Spalart-Allmaras, $k-\omega$ SST 1994, $k-\sqrt{k}L$ and $k-\omega$ TNT EARSM. In this case, the main goal is to discuss the numerical accuracy of the prediction of scale-effects which is illustrated for the form-factor, $1+K$, and the wake-fraction, W_F.

The remaining of this paper is structured as follows: Section 2 describes the main features of the selected turbulence models. The flow solver, computational domain and boundary conditions, grid sets, numerical settings and the procedures to estimate the modelling error are presented in Section 3. Results and their discussion are presented in Section 4 and conclusions are summarized in Section 5.

2. Mathematical model

The application of time-averaging to the continuity and momentum equations leads to the RANS equations that may be written[3] for incompressible and one-phase flow as

$$\frac{\partial V_i}{\partial x_i} = 0, \tag{1}$$

and

$$V_j\frac{\partial V_i}{\partial x_j} = -\frac{1}{\rho}\frac{\partial P}{\partial x_i} + \frac{\partial}{\partial x_j}\left[\nu\left(\frac{\partial V_i}{\partial x_j} + \frac{\partial V_j}{\partial x_i}\right)\right] + \frac{1}{\rho}\frac{\partial \tau_{ij}}{\partial x_j}, \tag{2}$$

where x_i are the coordinates of a Cartesian coordinate system, V_i are the time-averaged Cartesian velocity components, P is the time-averaged pressure, ρ is the fluid density, ν the fluid kinematic viscosity, and τ_{ij} is the Reynolds stresses tensor. Equations (1) and 2 require a turbulence model to determine τ_{ij} and become a closed system of equations.

2.1. Turbulence models

In this work we have used fourteen different turbulence models (some widely used in hydrodynamics) that are applicable in the viscous sub-layer (down to the wall) and use two different approaches to determine τ_{ij}:

- The Boussinesq assumption that leads to the concept of isotropic eddy-viscosity ν_t

$$\frac{\tau_{ij}}{\rho} = 2\nu_t S_{ij} - \frac{2}{3}k\delta_{ij}, \tag{3}$$

where k is the turbulence kinetic energy and the strain-rate tensor is defined by

$$S_{ij} = \frac{1}{2}\left(\frac{\partial V_i}{\partial x_j} + \frac{\partial V_j}{\partial x_i}\right). \tag{4}$$

- EARSM are non-linear two-equation models that determine the Reynolds stresses from

$$\frac{\tau_{ij}}{\rho} = -a_{ij} - \frac{2}{3}k\delta_{ij}, \tag{5}$$

where a_{ij} is the anisotropy tensor that is a function of S_{ij}, k, specific dissipation, ω, velocity invariants, and vorticity tensor

$$\Omega_{ij} = \frac{1}{2}\left(\frac{\partial V_i}{\partial x_j} - \frac{\partial V_j}{\partial x_i}\right). \tag{6}$$

Although EARSM models are anisotropic models, this type of formulation requires an underlying isotropic model (Wallin and Johansson, 2000).

The main features of the selected turbulence models are presented below.[4]

2.1.1. One-equation Eddy-Viscosity models

We have selected three eddy-viscosity one-equation models:

- The Spalart-Allmaras model (SA) (Spalart and Allmaras, 1992) that determines ν_t from

$$\nu_t = \tilde{\nu} f_{\nu_1}, \tag{7}$$

where f_{ν_1} is a damping function, and the dependent variable of the model $\tilde{\nu}$ is determined from the following transport equation[5]:

$$V_i\frac{\partial \tilde{\nu}}{\partial x_i} = c_{b_1}\tilde{\nu}\tilde{S} + \frac{1}{\sigma}\left(\frac{\partial}{\partial x_j}\left[(\nu+\tilde{\nu})\frac{\partial \tilde{\nu}}{\partial x_j}\right] + c_{b_2}\frac{\partial \tilde{\nu}}{\partial x_i}\frac{\partial \tilde{\nu}}{\partial x_i}\right) - c_{w_1}f_w\left(\frac{\tilde{\nu}}{d}\right)^2, \tag{8}$$

where d is the distance to the wall.

- A model proposed by Menter (MT) (Menter, 1997) that is derived from the $k-\varepsilon$ model (Launder and Sharma, 1974) and does not require the distance to the wall. The eddy-viscosity also uses a damping function D_2

$$\nu_t = \tilde{\nu}_t D_2, \tag{9}$$

and $\tilde{\nu}_t$ is calculated from the following transport equation

$$V_i\frac{\partial \tilde{\nu}_t}{\partial x_i} = c_1 D_1 \tilde{\nu}_t S + \frac{\partial}{\partial x_j}\left[\left(\nu + \frac{\tilde{\nu}_t}{\sigma}\right)\frac{\partial \tilde{\nu}_t}{\partial x_j}\right] - c_2 E_{1_e}, \tag{10}$$

where S is the trace of the strain-rate tensor.

- The $\sqrt{k}L$ (SKL) model proposed in Menter et al. (2006) that determines the eddy-viscosity from

$$\nu_t = c_\mu^{1/4}\phi. \tag{11}$$

The dependent variable, $\phi = \sqrt{k}L$, is obtained from the solution of

$$V_i\frac{\partial \phi}{\partial x_i} = \frac{\phi}{k}\nu_t S^2\left[\zeta_1 - \zeta_2\left(\frac{L}{L_{\nu_K}}\right)\right] + \frac{\partial}{\partial x_j}\left[\left(\nu + \frac{\phi}{\sigma_\phi}\right)\frac{\partial \phi}{\partial x_j}\right] - \zeta_3 k - 6\nu\frac{\Phi}{d^2}f_\phi, \tag{12}$$

with k determined from the equilibrium assumption

$$k = \nu_t\frac{S}{\sqrt{c_\mu}}. \tag{13}$$

Eq. (13) is also used with the SA and MT models to determine k.

2.1.2. Two-equation Eddy-Viscosity models

We have selected one Low-Reynolds version of the $k-\varepsilon$ model Abe et al. (1994), six versions of the $k-\omega$ model Wilcox (1988, 1998), Kok (2000), Menter (1994, 2003), and the $k-\sqrt{k}L$ model (Menter et al., 2006).

The Abe-Kondoh-Nagano (AKN) Low-Reynolds $k-\varepsilon$ model deter-

[3] Diffusion term could be simplified with the continuity equation, but the general form of the term is more appropriate for turbulence models based on the eddy-viscosity.

[4] Constants and functions of the models are not presented.

[5] The tripping term of the original SA model (Spalart and Allmaras, 1992) is neglected ($f_{t_2} = 0$).

mines the eddy-viscosity from

$$\nu_t = c_\mu f_\mu \frac{k^2}{\varepsilon}, \tag{14}$$

with the transport equations of k and of the dissipation rate of turbulence kinetic energy, ε, given by

$$V_i\frac{\partial k}{\partial x_i} = \nu_t S^2 + \frac{\partial}{\partial x_j}\left[\left(\nu + \frac{\nu_t}{\sigma_k}\right)\frac{\partial k}{\partial x_j}\right] - \varepsilon, \tag{15}$$

$$V_i\frac{\partial \varepsilon}{\partial x_i} = c_{\varepsilon 1}\nu_t S^2\frac{\varepsilon}{k} + \frac{\partial}{\partial x_j}\left[\left(\nu + \frac{\nu_t}{\sigma_\varepsilon}\right)\frac{\partial \varepsilon}{\partial x_j}\right] - c_{\varepsilon 2}f_{\varepsilon 2}\frac{\varepsilon^2}{k}. \tag{16}$$

This model may exhibit undesirable pseudo-laminar solutions (Rumsey et al., 2006) for flows that include transition from laminar to turbulent regime. To avoid this problem, the limiter of $f_{\varepsilon 2}$ proposed in Rumsey et al. (2006) is applied in the initial iterations of the calculations performed with the AKN model.

The Wilcox (1988) and Wilcox (1998) (W88 and W98), the Turbulent Non-Turbulent (TNT) Kok (2000) and the baseline (BSL) Menter (1994) versions of the $k-\omega$ model calculate the eddy-viscosity from

$$\nu_t = \frac{k}{\omega}, \tag{17}$$

where $\omega \propto \varepsilon/k$. The k and ω transport equations are given by

$$V_i\frac{\partial k}{\partial x_i} = \nu_t S^2 + \frac{\partial}{\partial x_j}\left[\left(\nu + \frac{\nu_t}{\sigma_k}\right)\frac{\partial k}{\partial x_j}\right] - \beta^*\omega k, \tag{18}$$

and

$$V_i\frac{\partial \omega}{\partial x_i} = \alpha S^2 + \frac{\partial}{\partial x_j}\left[\left(\nu + \frac{\nu_t}{\sigma_\omega}\right)\frac{\partial \omega}{\partial x_j}\right] + F_\omega\frac{\partial k}{\partial x_j}\frac{\partial \omega}{\partial x_j} - \beta\omega^2. \tag{19}$$

These four versions of the $k-\omega$ model use different constants and auxiliary functions that can be found in the references given above.

The Shear-Stress Transport (SST94) Menter (1994) and (SST03) Menter (2003) versions of the $k-\omega$ introduced a limiter to the eddy-viscosity that is defined by

$$\nu_t = \frac{a_1 k}{\max(a_1\omega; \Lambda F_2)}, \tag{20}$$

where Λ is the trace of the vorticity tensor Ω for SST94 and $\Lambda = S$ for SST03.

As the one-equation SKL model, the two-equation $k-\sqrt{k}L$ model (KSKL) is proposed in Menter et al. (2006). The model includes equation (12 and a transport equation for k that is given by

$$V_i\frac{\partial k}{\partial x_i} = \nu_t S^2 + \frac{\partial}{\partial x_j}\left[\left(\nu + \frac{\nu_t}{\sigma_k}\right)\frac{\partial k}{\partial x_j}\right] - c_\mu^{3/4}\frac{k^{3/2}}{L} - 2\nu\frac{k}{d^2}. \tag{21}$$

The eddy viscosity is given by

$$\nu_t = \min\left\{c_\mu^{1/4}\Phi; \frac{a_1 k}{S}\right\}. \tag{22}$$

2.1.3. Explicit algebraic Reynolds-stresses models

The EARSM models tested in this work follow the framework proposed in Wallin and Johansson (2000). The models presented in Hellsten (2005) are based on the BSL $k-\omega$ model and determine τ_{ij} from an effective eddy-viscosity and a corrective extra-anisotropy tensor $a_{ij}^{(ex)}$,

$$\nu_t = C_\mu k\tau, \tag{23}$$

and

$$\frac{\tau_{ij}}{\rho} = 2\nu_t S - \frac{2}{3}k\delta_{ij} - a_{ij}^{(ex)}k. \tag{24}$$

The two versions tested differ only in the definition of τ. For the option proposed in Wallin and Johansson (2000) (EARSM[1])

$$\tau^{-1} = \max(\beta^*\omega; \sqrt{k\omega/\nu}/6), \tag{25}$$

whereas the alternative (EARSM[2]) uses

$$\tau^{-1} = \beta^*\omega. \tag{26}$$

The third EARSM model tested follows a similar approach, but it is based on the TNT $k-\omega$ model (EARSM[3]). τ is defined from Eq. (26).

3. Problem setup

3.1. ReFRESCO solver

ReFRESCO (ReFRESCO, 2016) is a community based open-usage CFD code for the maritime world. It solves multiphase incompressible viscous-flows using the continuity and Navier-Stokes equations (filtered), complemented with turbulence models, cavitation models and volume-fraction transport equations for different phases. The equations are discretized using a finite-volume approach with cell-centred collocated variables, in strong-conservation form, and a pressure-correction equation based on the SIMPLE algorithm is used to ensure mass conservation. Time integration is performed implicitly with first or second-order backward schemes. At each implicit time step, the non-linear system for velocity and pressure is linearised with Picard's method and either a segregated or coupled approach is used. A segregated approach is adopted for the solution of all other transport equations.

The implementation is face-based, which permits grids with elements consisting of an arbitrary number of faces (hexahedrals, tetrahedrals, prisms, pyramids, etc.), and if needed h-refinement (hanging nodes). For turbulence modelling, RANS, SAS, DES, XLES, and PANS approaches can be used (LES is being currently studied) (Pereira et al., 2015a, 2015b). State-of-the-art CFD features such as moving, sliding and deforming grids, as well automatic grid adaptation (refinement and/or coarsening) are also available. Coupling with structural equations-of-motion is also possible. The code is parallelized using MPI and subdomain decomposition, and runs on Linux workstations and HPC clusters. The code is currently being developed, verified and tested at MARIN (the Netherlands) in collaboration with Instituto Superior Técnico (Portugal) and other universities around the world (see ReFRESCO, 2016).

3.2. Domain and boundary conditions

The flow around the KVLCC2 is calculated in a prismatic rectangular domain defined in a Cartesian coordinate system[6] (x_1, x_2, x_3) with the x_1 axis coincident with the keel line (pointing to the bow), the transverse x_2 axis perpendicular to the symmetry plane of the ship and the vertical x_3 axis forming a right-handed system as depicted in Fig. 2. The Reynolds number, $Re = V_\infty L_{pp}/\nu$, based on the incoming flow velocity, V_∞, and the distance between perpendiculars, L_{pp}, of the ship is equal to $Re = 4.60 \times 10^6$ at model-scale and $Re = 2.03 \times 10^9$ at full-scale (Fig. 3).

The computational domain includes the following boundaries: the surface and the symmetry plane ($x_2 = 0$) of the ship; the still water[7] plane located at $x_3 = 0.065L_{pp}$; the inlet and outlet planes located at $x_1 = \pm 2L_{pp}$; the lateral plane located at $x_2 = L_{pp}$ and the bottom plane placed at $x_3 = -L_{pp}$. The location of the boundaries is based on the

[6] The origin of the coordinate system is on the symmetry plane of the ship at the intersection of the keel line and aft perpendicular.

[7] The effect of the free-surface is neglected.

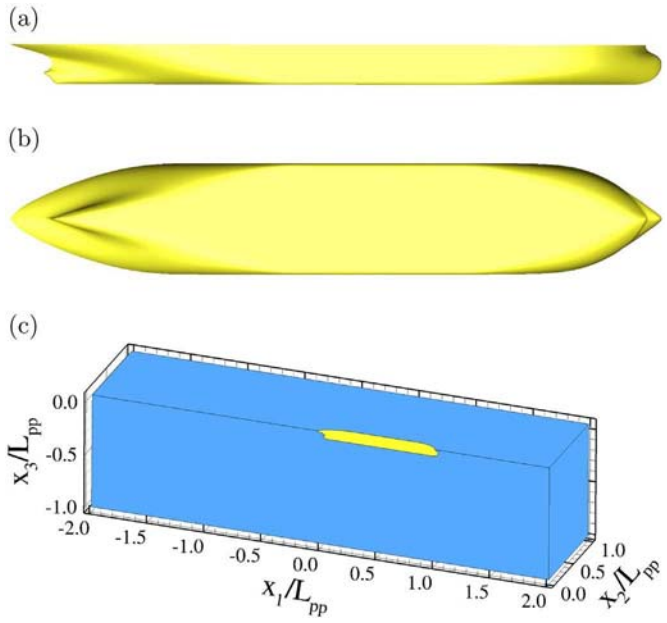

Fig. 2. KVLCC2 hull and computational domain views. (a) KVLCC2 hull - side view. (b) KVLCC2 hull - keel view. (c) Computational domain view.

sensitivity studies reported in Eça and Hoekstra (2009a). The KVLCC2 geometry[8] and the computational domain are illustrated in Fig. 2.

The following boundary conditions are applied at model and full-scale Reynolds number:

- On the ship surface, the velocity components are set equal to zero due to the impermeability and no-slip conditions. Shear-stress at the wall is determined directly from its definition (the dimensionless distance to the wall of the nearest cell centre $y^+_{c_2}$ is always lower than one), i.e. wall-functions[9] are not applied at both Reynolds numbers to avoid extra modelling errors (Eça et al., 2015). The normal derivative of the pressure is assumed to be equal to zero and all turbulence quantities are equal to zero except ε and ω. The ε wall value is given by $\varepsilon_{c_2} = 2\nu k_{c_2}/d^2_{c_2}$, where d designates the normal distance to the wall and $_{c2}$ the centre of the nearest-wall cell (Abe et al., 1994). ω is specified at the centre of the nearest-wall cell (Eça and Hoekstra, 2004) using $\omega_{c_2} = 6/(\beta d^2_{c_2})$ (Wilcox, 1998);
- Symmetry conditions are naturally applied at the symmetry plane of the ship, $x_2 = 0$; the effect of the free-surface is neglected and so symmetry conditions are also applied at the still water surface $x_3 = 0.065L_{pp}$;
- Velocity components are set equal to undisturbed flow conditions at the inlet, $x_1 = 2L_{pp}$, i.e. $V_1 = V_\infty$, $V_2 = 0$, $V_3 = 0$, and the pressure is extrapolated from the interior of the domain. All turbulence flow

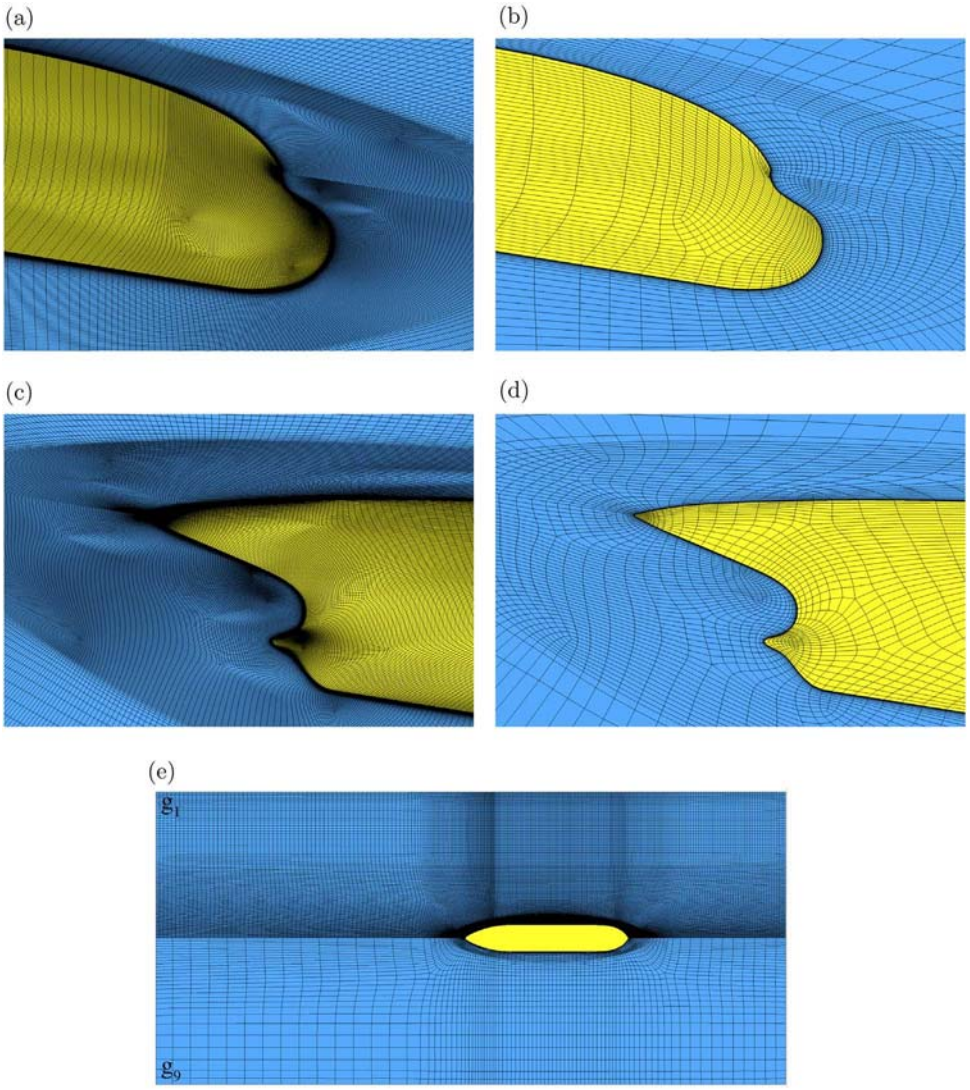

Fig. 3. Details and comparison of the finest g_1 and coarsest g_9 grids for the model-scale Reynolds number calculations. (a) Finest grid g_1 - bow view. (b) Coarsest grid g_9 - bow view. (c) Finest grid g_1 - stern view. (d) Coarsest grid g_9 - stern view. (e) Finest g_1 and coarsest g_9 grids at the still water plane.

quantities are specified using the turbulence intensity, I, and the ratio between the eddy and kinematic viscosities, ν_t/ν. For model-scale simulations $I = 1\%$ and $\nu_t/\nu = 0.1$, whereas $I = 10\%$ and $\nu_t/\nu = 10$ for full-scale calculations[10];

- At the outlet plane, $x_1 = -2L_{pp}$, all derivatives with respect to x_1 are set equal to zero;
- At the bottom of the computational domain, $x_3 = -L_{pp}$, a free-slip condition is applied and the derivatives of all turbulence quantities with respect to x_3 are set equal to zero;
- The pressure is imposed (P=0) at the lateral boundary, $x_2 = L_{pp}$, and the derivatives of the remaining dependent variables with respect to x_2 are set equal to zero.

3.3. Grid sets

Two sets of multi-block structured grids were generated for the selected computational domain. The two sets have a similar topology. However, the clustering of grid cells in the near-wall region is tuned for each Reynolds number to obtain a dimensionless distance[11] to the wall of the nearest cell centre $y^+_{c_2}$ below one, $y^+_{c_2} < 1$.

The grid refinement ratio $r_i = (N_c(g_1)/N_c(g_i))^{1/3}$, the number of cells N_c, and the values of $(y^+_{c_2})_{\max}$ obtained with the SST94 are summarized in Table 1, and Fig. 2 illustrates the finest g_1 and coarsest g_9 grids for the model-scale calculations. Naturally, full-scale grids are coarser than those for model-scale in the outer region of the flow due to the similar values of N_c and $y^+_{c_2}$.

3.4. Numerical settings

For all the simulations performed in this study, a segregated approach is adopted to solve the momentum, continuity and turbulence quantities transport equations. In order to guarantee that round-off and iterative errors are negligible when compared to discretization errors, all calculations are performed in double-precision (14 digits) and the iterative convergence criteria c_{it} requires that the L_∞ norm (maximum value) of the normalized residual[12] of all transport equations is smaller than 10^{-8}. The influence of c_{it} on the numerical uncertainty of the predicted resistance coefficients is illustrated in Section 4.1.1.

All discretization schemes are second-order accurate with the exception of the convective terms of the turbulence quantities transport equations that are approximated by first-order Upwind. Nonetheless, simulations were also performed for the SST94 model with second-order schemes for the convective terms of the turbulence quantities. The results showed that the numerical uncertainty of mean flow quantities was similar to that obtained with first-order Upwind in the k and ω transport equations. On the other hand, second-order schemes make iterative convergence more troublesome and so first-order Upwind is adopted for all turbulence models.

3.5. Estimation of modelling errors

Modelling errors are estimated with the procedures proposed in The American Society of Mechanical Engineers (2009, 2016). For a selected flow quantity ϕ (local or functional), the interval that contains the modelling error δ_ϕ for 95 out of 100 cases is given by

Table 1
Properties of the grid sets used in the simulations at model ($Re = 4.60 \times 10^6$) and full-scale ($Re = 2.03 \times 10^9$): grid refinement ratio, r_i, number of cells, N_c, and maximum and average $y^+_{c_2}$ at the ship's hull (using the SST94 model), $(y^+_{c_2})_{\max}$ and $\bar{y}^+_{c_2}$.

Grid	Re=4.60×10^6				Re=2.03×10^9			
	r_i	N_c	$(y^+_{c_2})_{\max}$	$\bar{y}^+_{c_2}$	r_i	N_c	$(y^+_{c_2})_{\max}$	$\bar{y}^+_{c_2}$
g_1	1.00	20,140,032	0.191	0.110	1.00	20,975,616	0.157	0.100
g_2	1.14	13,472,256	0.221	0.129	1.14	14,058,688	0.181	0.117
g_3	1.33	8,506,368	0.261	0.149	1.33	8,858,880	0.213	0.139
g_4	1.60	4,913,600	0.311	0.182	1.60	5,104,000	0.258	0.171
g_5	2.00	2,508,800	0.404	0.231	2.00	2,613,248	0.325	0.218
g_6	2.43	1,401,023	0.453	0.271	2.43	1,459,393	0.376	0.259
g_7	2.87	852,841	0.538	0.323	2.86	894,751	0.436	0.306
g_8	3.50	470,331	0.672	0.401	–	–	–	–
g_9	4.46	227,115	0.869	0.502	–	–	–	–

$$E_\phi - U_{val} \le \delta_\phi \le E_\phi + U_{val}, \tag{27}$$

where the comparison error, $E_\phi = S_\phi - D_\phi$, is the difference between the simulated result, S_ϕ, and the experimental measurement, D_ϕ, and U_{val} is the Validation uncertainty.

U_{val} is a consequence of the fact that neither S_ϕ or D_ϕ are exact values, i.e. there are numerical U_S and experimental U_D uncertainties. Furthermore, there are several parameters included in the problem definitions that are not exact, as for example the turbulence quantities used to define the inlet conditions or the properties of the fluid that depend on its temperature. Therefore, we also have an "input" uncertainty U_I. Assuming that these uncertainties are independent, we obtain

$$U^2_{val} = U^2_S + U^2_D + U^2_I. \tag{28}$$

In this work, U_S is estimated with the procedure proposed in Eça and Hoekstra (2014), U_D is obtained from the papers that describe the experiments (Kim et al., 2001; Lee et al., 2003), and U_I is assumed[13] to be zero.

Recently, a multivariate metric based on the work presented in Hills (2006) has been proposed in The American Society of Mechanical Engineers (2016) to quantify the modelling error for multiple set points, as for example all the experimental measuring locations at the propeller plane of the KVLCC2 tanker (Kim et al., 2001; Lee et al., 2003).

The metric r for N evaluations of E_ϕ and U_{val} is defined by

$$r = \sqrt{\mathbf{E}^T \mathbf{V}^{-1}_{val} \mathbf{E}}, \tag{29}$$

where $\mathbf{E}$ is a vector containing the N values of E_ϕ, and $\mathbf{V}_{val}$ is the covariance matrix which for $U_I = 0$ is a diagonal matrix containing $U^2_{val} = U^2_S + U^2_D$. If the uncertainties in the N estimated δ_ϕ are represented by normal distributions, the expected value of r is obtained from a χ^2 distribution that leads to a reference value, r_{ref}, given by the expected value plus the standard uncertainty (Hills, 2006).

$$r_{ref} = \sqrt{N + \sqrt{2N}}, \tag{30}$$

If r/r_{ref} is clearly larger than one, there is evidence that the simulations are not a consistent representation of the experimental observations. On the other hand, r/r_{ref} smaller than one must be interpreted taking into account the level of U_{val} that is weighting the multivariate metric.

4. Results

This section includes three different exercises:

[8] The transom of the stern has been faired. Such approach avoids problems of having statistical unsteady flows due to vortex shedding in wake separated regions.

[9] Unlike other studies, like for example Khor and Xiao (2011), Demirel et al. (2014)

[10] ν_t/ν is increased to maintain similar inflow conditions among model and full-scale Reynolds number simulations.

[11] Friction velocity and kinematic viscosity of the fluid are used to define the reference length.

[12] Normalized residuals are equivalent to variable changes in a simple Jacobi iteration.

[13] The estimation of U_I is extremely time consuming and practically not feasible for the present exercise. Furthermore, there is no information about the uncertainty of the specified inlet quantities and/or fluid properties.

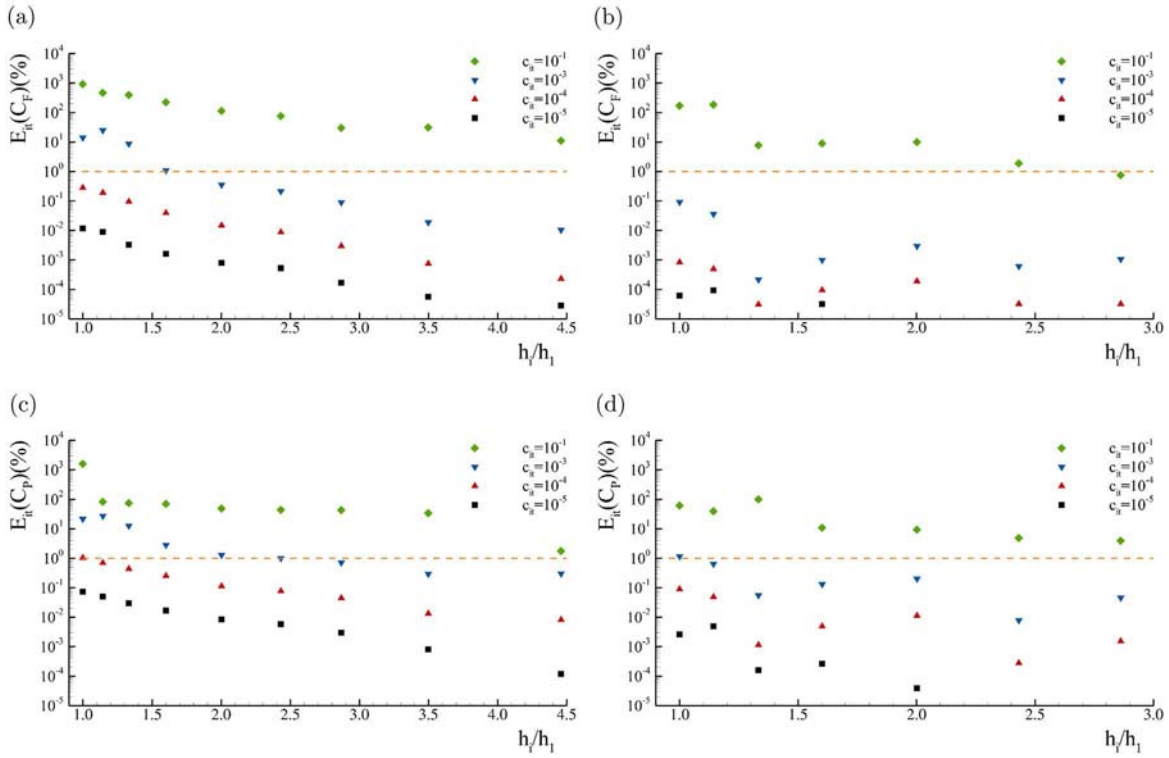

Fig. 4. Estimate of the iterative error of the friction and pressure resistance coefficients, C_F and C_P, at model and full-scale Reynolds numbers using different iterative convergence criteria, c_{it}. Reference values are obtained for $c_{it} = 10^{-8}$. Results obtained with the SST94 turbulence model. (a) C_F at model-scale. (b) C_F at full-scale. (c) C_P at model-scale. (d) C_P at full-scale.

(1) Solution Verification to determine the numerical uncertainty of the selected flow quantities of the flow around the KVLCC2 tanker at model and full-scale Reynolds numbers;
(2) Validation procedure to quantify the modelling error of the selected flow quantities at model-scale Reynolds number;
(3) Determination of scale-effects with different turbulence models.

The selected flow quantities for the first two exercises are the resistance coefficient C_T and the mean velocity components and turbulence kinetic energy at the propeller plane. In the latter case, we have analysed the influence of the Reynolds number on the form-factor $1+K$ and wake-fraction W.

4.1. Solution verification

The goal of a Solution Verification exercise is to determine the numerical uncertainty of a given simulation, which is a consequence of round-off, iterative and discretization errors (Roache, 2009). All the simulations were performed in double precision and so round-off errors are negligible when compared to the discretization error. On the other hand, a reliable estimate of discretization errors requires iterative errors one to two orders of magnitude below the discretization error (Eça and Hoekstra, 2009b). Therefore, it is necessary to select an iterative convergence criteria that guarantees a negligible contribution of the iterative error to the numerical uncertainty.

4.1.1. Iterative errors

In the present simulations, the iterative convergence is controlled by the maximum normalized residual (L_∞ norm) of all transport equations solved, c_{it}, which is equivalent to the largest dimensionless variables change in a simple Jacobi iteration. In order to assess the level of the iterative error, we have performed simulations with the SST94 turbulence model for model and full-scale Reynolds numbers with 5 different values of c_{it}: 10^{-1}, 10^{-3}, 10^{-4}, 10^{-5} and 10^{-8}. Fig. 4 presents the differences between the friction C_F and pressure C_P resistance coefficients obtained with the different values of c_{it} tested, $E_{it}(C_F)$ and $E_{it}(C_P)$. The reference results are those obtained with $c_{it} = 10^{-8}$ and the estimates of the iterative error of C_F and C_P are presented as a function of the grid refinement level h_i/h_1. The dashed lines depicted in the plots corresponds to $E_{it} = 1\%$.

As experienced before (Eça and Hoekstra, 2009b), for the same level of c_{it}, the influence of the iterative error increases with grid refinement. The data show that $c_{it} = 10^{-5}$ may not guarantee iterative errors two orders of magnitude smaller than the discretization errors and so we have adopted $c_{it} = 10^{-8}$ for all calculations. It is also clear that the "classical" three orders of magnitude of residual drop as iterative convergence criteria can lead to significant iterative errors (close to 10% for the finest grids of the model-scale simulations) even using the L_∞ norm of the residual.

Naturally, the decrease of c_{it} leads to an increase of the number of iterations N_{it} required to satisfy the iterative convergence criteria. This effect is illustrated in Fig. 5 that presents the L_∞ and L_2 norms of the residuals of the x_1 momentum equation (designated by V_1) along the N_{it} iterations required to satisfy the iterative convergence criteria at model and full-scale Reynolds numbers in the finest grids g_1. There is approximately a difference of two orders of magnitude between the L_∞ and L_2 norms of the normalized residuals for the two simulations.

4.1.2. Discretization errors

Discretization errors are estimated from grid refinement studies and numerical uncertainties are obtained with the procedure proposed[14] in Eça and Hoekstra (2014), which assumes that the contribution of round-off and iterative errors to the numerical uncertainty is negligible.

The resistance coefficient C_T is obtained from the sum of the friction C_F and pressure C_P resistance coefficients and so formally

[14] For monotonic convergence the estimated uncertainties are similar to those determined by the Grid Convergence Index (Roache, 1998) or Factor of Safety Method (Xing and Stern, 2010).

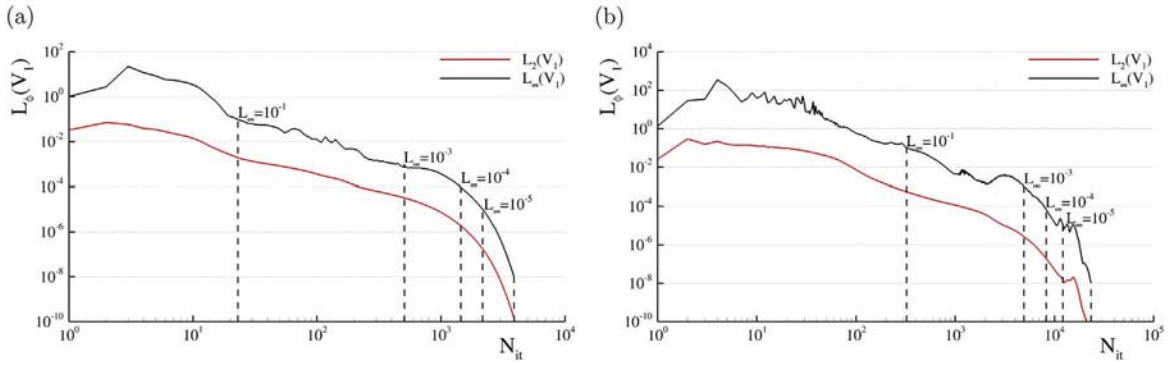

Fig. 5. Stream-wise velocity, V_1, residual history in the simulations at model and full-scale Reynolds numbers for grid g_1. Results obtained with the SST94 turbulence model. (a) Model-scale. (b) Full-scale.

Table 2
Friction C_F, pressure C_P and total C_T resistance coefficients with respective numerical uncertainties obtained at model-scale Reynolds number $Re = 4.6 \times 10^6$ in the finest g_1. Reference value for U_{C_T} is the experimental result.

Model	$C_P \times 10^3$	U_{C_P}(%)	$C_F \times 10^3$	U_{C_F}(%)	$C_T \times 10^3$	U_{C_T}(%)
SA	0.578	2.17	3.446	0.39	4.024	0.63
MT	0.619	2.32	3.477	0.47	4.096	0.75
SKL	0.627	1.57	3.292	1.33	3.919	1.30
AKN	0.580	8.75	3.540	3.26	4.120	4.04
W88	0.578	4.82	3.613	1.45	4.191	1.95
W98	0.706	5.29	3.208	1.57	3.914	2.13
BSL	0.653	0.43	3.501	1.34	4.154	1.21
SST94	0.680	1.07	3.381	1.71	4.061	1.58
SST03	0.675	0.95	3.383	1.65	4.058	1.51
TNT	0.660	4.00	3.474	1.11	4.134	1.58
EARSM[1]	0.813	3.56	3.579	6.31	4.392	6.20
EARSM[2]	0.824	0.61	3.478	2.11	4.302	1.91
EARSM[3]	0.771	4.76	3.195	1.07	3.966	1.72
KSKL	0.656	2.21	3.328	0.85	3.984	1.04

$U_{C_T} = U_{C_F} + U_{C_P}$. Table 2 presents the estimated values of U_{C_F} and U_{C_P} for the finest grid g_1 of the model-scale simulations. The discretization error is estimated from the results obtained in the 5 finest grids ($1 \le h_i/h_1 \le 2$), which range from 20.1×10^6 to 2.5×10^6 cells. The convergence properties of C_F and C_P are illustrated in Fig. 6 that presents also the estimated orders of grid convergence p and the error bars of the finest grid solutions. The numerical uncertainty of C_T, U_{C_T}, is also presented in Table 2 in percentage of the experimental result $C_T = 4.11 \times 10^{-3}$. The main remarks suggested by the data presented in Table 2 and Fig. 6 are:

- The numerical convergence properties of C_F and C_P (observed order of grid convergence p and error constant) are strongly dependent on the selected turbulence model. There are turbulence models that lead to monotonic convergence with p ranging from 1.06 to 1.92, models that lead to $p > 2$ and so p is set equal to 2 ($p' = 2$), and models that do not exhibit monotonic convergence for $1 \le h_i/h_1 \le 2$, which leads to the need to use two terms expansions to estimate the exact solution (Eça and Hoekstra, 2014). In these cases, the estimated uncertainties are penalized but still comparable to those obtained for the "well-behaved" data;
- For a given turbulence model, the convergence properties obtained for C_F and C_P are almost never identical. Furthermore, when both variables exhibit monotonic convergence the observed order of grid convergence of C_F and C_P is most of the times different. Nonetheless, for the present level of grid refinement, it is clearly more difficult to estimate the observed order of grid convergence for C_P than for C_F;
- In most of the turbulence models tested, the data obtained in the grids with $h_i/h_1 > 2$ is in good agreement with the fit performed for the grids with $h_i/h_1 \le 2$. The clear exception is the AKN model that shows an awkward shift in the data behaviour for the four finest grids, which is a consequence of a strange increase of the extension of laminar flow at the bow with grid refinement. In such conditions it is troublesome to make reliable estimates of the numerical uncertainty;
- Most of the values of U_{C_T} obtained for the finest grid are between 1% and 2%, which is still larger than the reported experimental uncertainty of 1%. The main exception is obtained for the EARSM[1] where the scatter observed in the data strongly penalizes the estimated uncertainties. Nevertheless, for most of the selected models, the values obtained for the finest grid g_1 are sufficiently small to assess the modelling error.

Uncertainty estimates were also performed for the mean velocity components and turbulence kinetic energy at all the locations of the propeller plane with available experimental measurements. The estimates were based on the data of the four finest grids covering a grid refinement ratio of 1.6. As for the force coefficients, the apparent convergence condition and the error constant depend on the selected turbulence model (and on the selected flow quantity). Nonetheless, there are trends that are observed for all 14 turbulence models tested and four selected flow quantities: the convergence is not monotonic for approximately 40% of the locations; in the remaining 60%, the observed order of grid convergence is between 1 and 2 only for 30% of the cases. As a consequence of these convergence properties, the estimated numerical uncertainties will probably be too conservative. However, the level of grid refinement required to obtain four data points with monotonic convergence at the majority of the experimental locations of the propeller plane would not be affordable for such exercise.

The convergence of C_F and C_P with grid refinement for the full-scale calculations is illustrated in Fig. 7. Table 3 presents the values of C_P, C_F and C_T obtained in the finest grid g_1 and the respective numerical uncertainties. For the four turbulence models tested there are again cases with non monotonic convergence (2 terms expansions) and cases where the exact solution is estimated with a fixed order of grid convergence ($p' = 2$ in the plots). Furthermore, for a given turbulence model the convergence properties obtained at model and full-scale are not always identical. The absolute values of U_{C_F} and U_{C_P} obtained at full-scale are similar to those obtained at model-scale. However, due to the reduction of C_T with the increase of Reynolds number the values of U_{C_T} in percentage become larger at full-scale than at model-scale.

4.2. Validation

The application of the ASME V & V 2009 Validation procedure (The American Society of Mechanical Engineers, 2009, 2016) to estimate

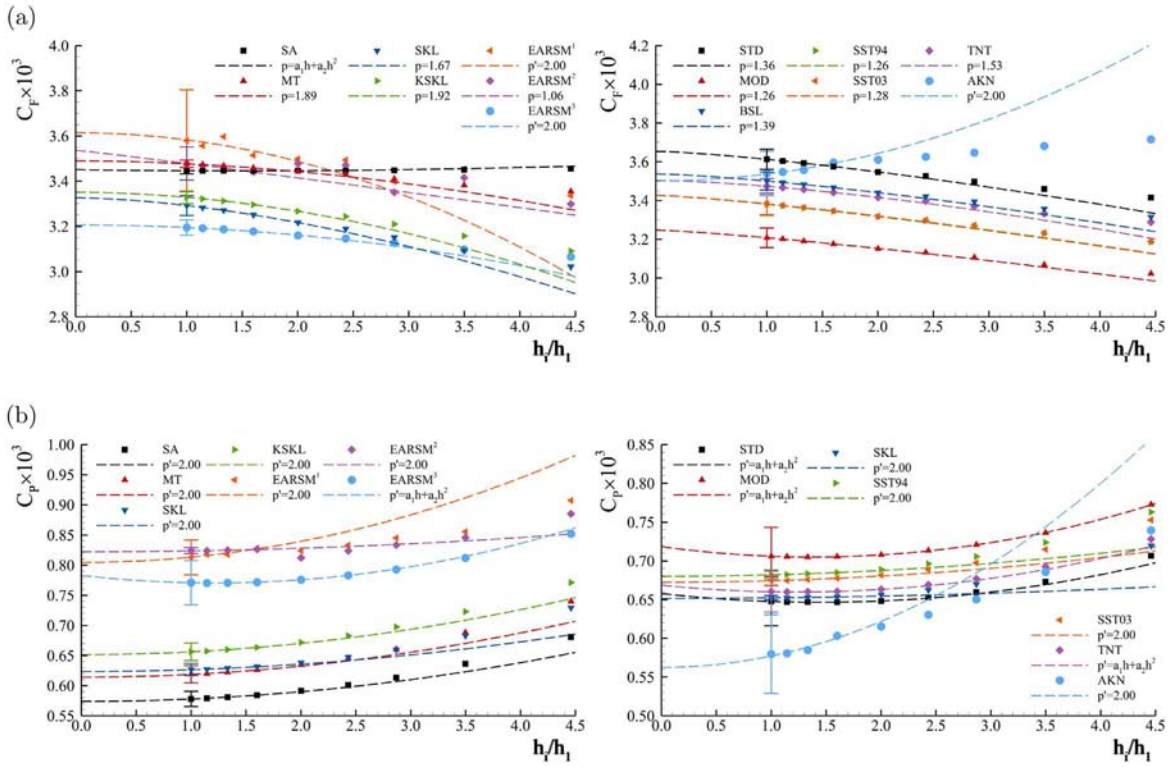

Fig. 6. Convergence of the friction and pressure coefficients C_F and C_P with the grid refinement for model-scale Reynolds number $Re = 4.6 \times 10^6$. Observed order of grid convergence is p. p' means that the order is fixed and $a_1h + a_2h^2$ means that convergence is not monotonic. (a) C_F. (b) C_P.

modelling errors requires experimental data and its uncertainties, numerical simulations and its uncertainties, and input parameter uncertainties. The input parameters uncertainty is assumed to be zero and the numerical solutions and its uncertainties have been presented in the previous section. Experimental data is obtained from the open literature and is presented in the following section.

4.2.1. Experimental data

The flow around the KVLCC2 tanker has been measured at model-scale Reynolds number (4.60×10^6) in a towing tank (Kim et al., 2001) and in a wind tunnel (Lee et al., 2003). The towing test was performed at Froude number of F_r=0.142 and the wind tunnel measurements were performed for a double body.

The (time-averaged) resistance coefficient C_T was only measured for the towing tank test (Kim et al., 2001) and the reported value is $C_T = 4.11 \times 10^{-3}$ with an estimated uncertainty of 1%. The mean velocity field at the propeller plane, $x_1 = 0.0175L_{pp}$, was measured with a pitot tube in Kim et al. (2001) and with a hot-wire anemometry in Lee et al. (2003). The uncertainties reported in Kim et al. (2001) for the mean velocity components are 1.2%, whereas the uncertainties given in Lee et al. (2003) are 0.5% for V_1, 0.7% for V_2, 1.0% for V_3 and 12.8% for the turbulence kinetic energy k. It must be mentioned that the asymmetry of the velocity field of both experiments is larger than the reported uncertainties. Nonetheless, we have used the values given in Kim et al. (2001) and Lee et al. (2003) for the estimation of U_{val}.

Table 3
Friction C_F, pressure C_P and total C_T resistance coefficients with respective numerical uncertainties obtained at full-scale Reynolds number $Re = 2.03 \times 10^9$ in the finest grid g_1.

Model	$C_P \times 10^3$	U_{C_P}(%)	$C_F \times 10^3$	U_{C_F}(%)	$C_T \times 10^3$	U_{C_T}(%)
SA	0.215	8.40	1.548	3.53	1.764	4.13
SST94	0.229	5.23	1.515	1.43	1.744	1.93
EARSM^3	0.263	6.38	1.424	1.99	1.686	2.68
KSKL	0.218	1.21	1.461	3.53	1.679	3.23

The two experiments have different boundary conditions. The free-surface is obviously present in the towing tank tests and blockage

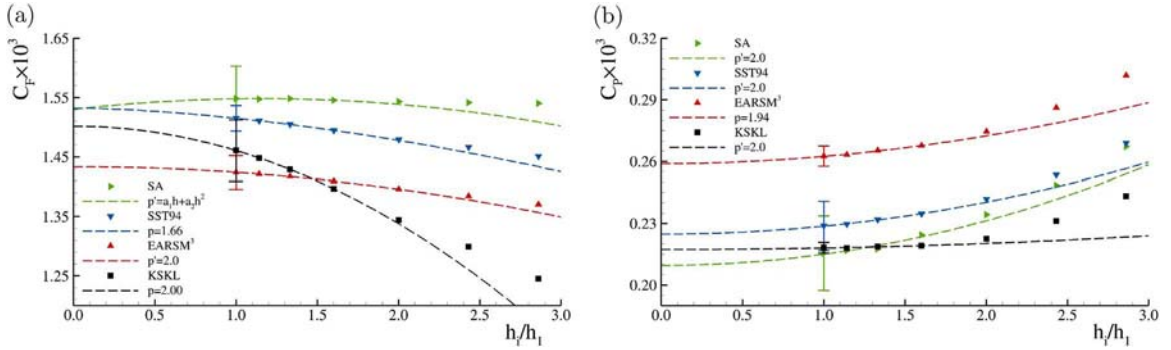

Fig. 7. Convergence of the friction and pressure coefficients C_F and C_P with the grid refinement for full-scale Reynolds number $Re = 2.03 \times 10^9$. Observed order of grid convergence is p. p' means that the order is fixed and $a_1h + a_2h^2$ means that convergence is not monotonic. (a) C_F. (b) C_P.

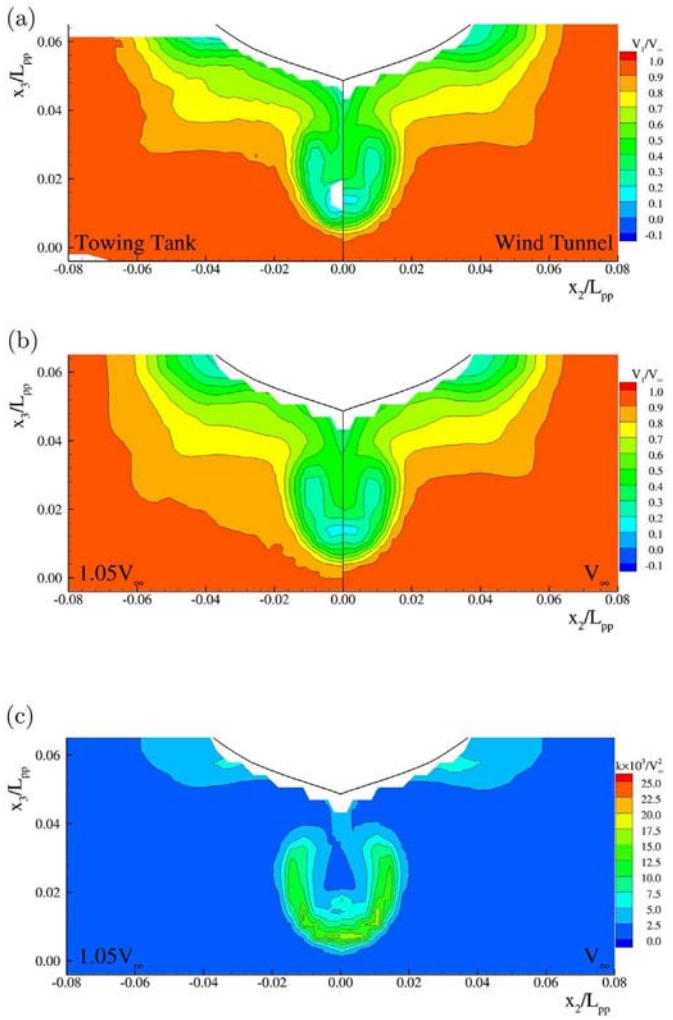

Fig. 8. Wind tunnel and towing tank stream-wise velocity, V_1, and turbulence kinetic energy, k, measurements. Wind tunnel results with ($V_{ref} = 1.05V_\infty$) and without (V_∞) correction of blockage effects. (a) Wind tunnel and towing tank V_1 measurements. (b) Wind tunnel and towing tank V_1 measurements ($V_{ref} = 1.05V_\infty$ and V_∞). (c) Wind tunnel k measurements ($V_{ref} = 1.05V_\infty$ and V_∞).

effects influence the wind tunnel experiments. In Larsson et al. (2013), it is suggested to correct the reference velocity of the incoming flow of the wind tunnel experiments to $1.05V_\infty$ to consider the blockage effect. The comparison of the V_1 and k isolines at the propeller plane with and without the blockage corrections is presented in Fig. 8. The figure also includes the comparisons of the stream-wise velocity field of the two tests. The results suggest that blockage effects are not negligible and not identical in the two facilities. Furthermore, the resistance coefficient measured in the towing tank includes wave resistance, which for F_r=0.142 is supposed to have a non-negligible contribution to the resistance (it may reach 4% of C_T for this test-case at model-scale Raven, 2016). Therefore, a rigorous Validation exercise would require simulations performed with different settings for each data set. However, such exercise would also require a significant amount of information that is not available from the experiments, as for example the inlet values of all the turbulence quantities included in the turbulence models tested in this exercise.

4.2.2. Modelling errors

The modelling errors δ_ϕ of the resistance coefficient, mean velocity components and turbulence kinetic energy at the propeller plane obtained with the fourteen turbulence models tested at model-scale Reynolds number are presented below. It must be emphasized that

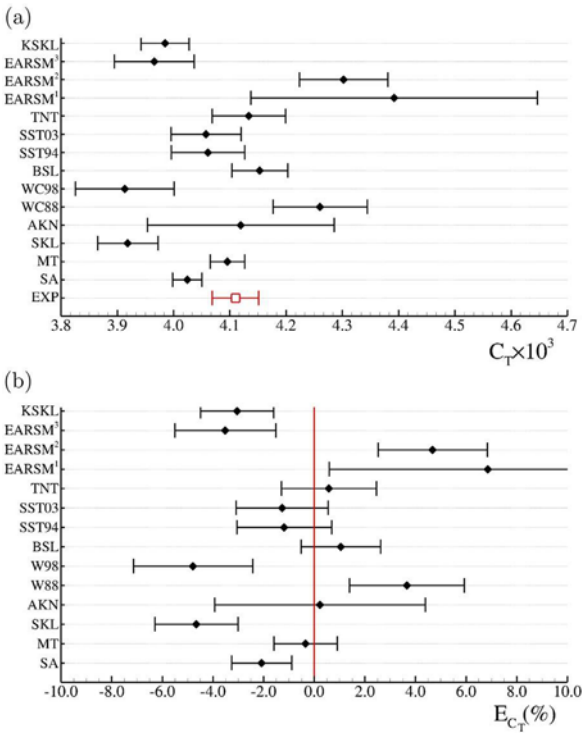

Fig. 9. Resistance coefficient, C_T, comparison error, E_{C_T}, and correspondent numerical and validation uncertainties, U_{C_T} and $U_{val}(C_T)$, obtained with the 14 turbulence models tested. (a) $C_T + U_{C_T}$. (b) $E_{C_T} + U_{val}$.

there are mismatches between the physical (experimental) and mathematical (simulations) models that make this exercise less rigorous than desirable. Namely, the differences in size between the computational domain, wind tunnel and towing tank; the fairing of the transom stern for the simulations and the absence of free-surface in the simulations. Furthermore, inlet conditions for the turbulence quantities in the simulations were prescribed without any knowledge of the experimental conditions. Nonetheless, it is worthwhile to perform this exercise using the data presented in Kim et al. (2001) and Lee et al. (2003) to illustrate the advantages of assessing quantitatively modelling errors over the traditional graphical comparisons between experiments and simulations.

The application of the procedure described in Section 3.5 to the results obtained for C_T is illustrated in Fig. 9, which presents the values obtained from the simulations with respective uncertainty in Fig. 9a and the comparison errors E_{C_T} and validation uncertainties in Fig. 9b. The data show that there is a significant influence of the turbulence model on the modelling error of the C_T prediction. The fourteen turbulence models tested lead to a range of values that corresponds to approximately 12% of the experimental result. Furthermore, there are significant differences between the U_{val} obtained for each turbulence model with values between 1 and 6%. We point out that the range of values obtained with the different turbulence models and their validation uncertainties is not dependent on the limitations of this exercise discussed above.[15] There are several models with overlapping intervals $[E_{C_T} - U_{val}, E_{C_T} + U_{val}]$, but there are changes in the same family of turbulence models that lead to non-overlapping intervals, as for example W88 and W98 or EARSM^1 and EARSM^2.

Fig. 10 presents the stream-wise velocity, V_1, and turbulence kinetic energy, k, fields obtained at the propeller plane, $x_1/L_{pp} = 0.0175$, with the 14 turbulence models tested. Typically, these plots are compared qualitatively with those presented in Fig. 8 corresponding to the

[15] A corrected value of the experimental data would only shift the error bars plotted in Fig. 9b horizontally.

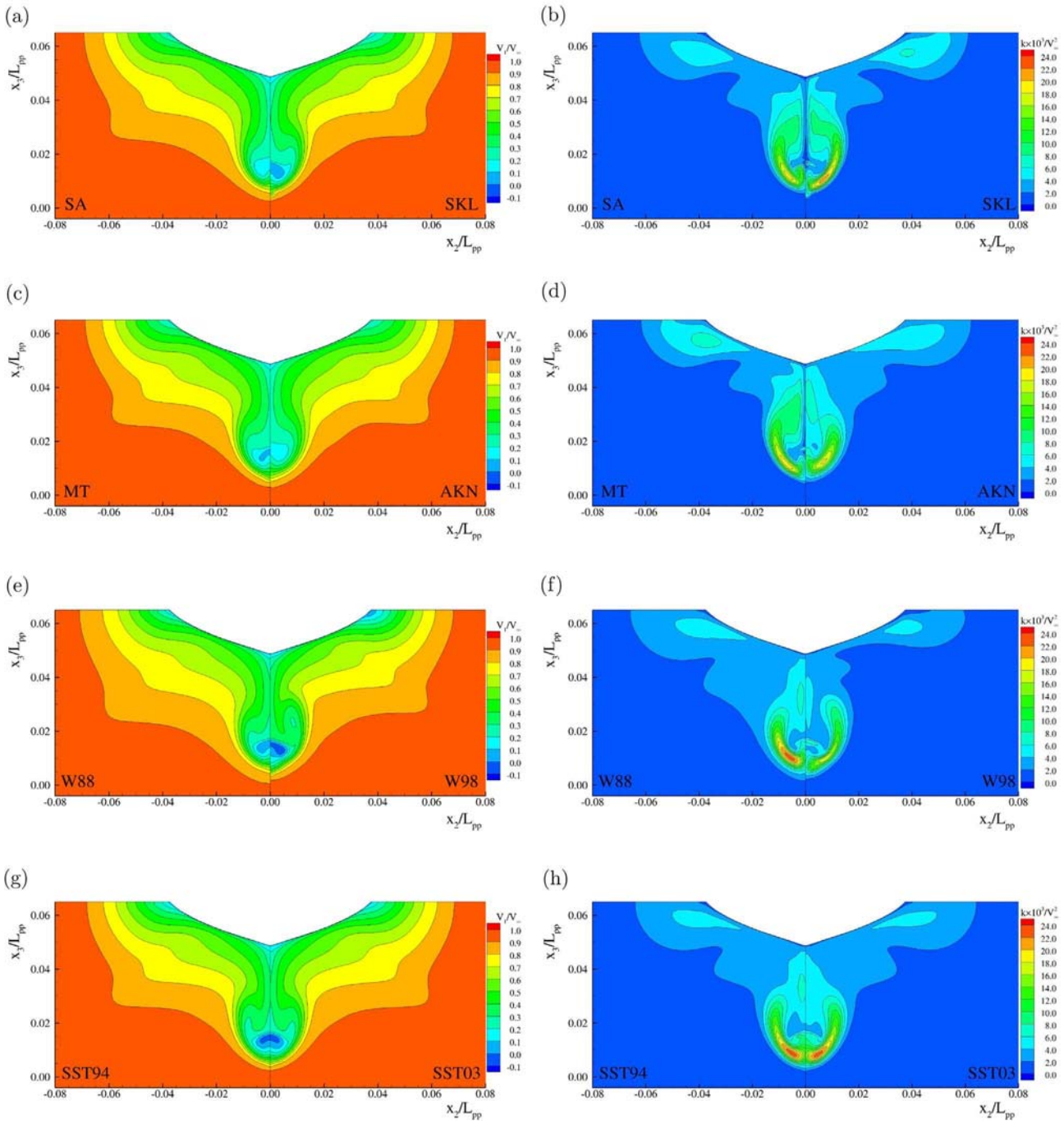

Fig. 10. Stream-wise velocity, V_1, and turbulence kinetic energy, k, fields at the propeller plane $x_1/L_{pp} = 0.0175$ obtained with the fourteen turbulence models tested. Stream-wise velocity, V_1, and turbulence kinetic energy, k, fields at the propeller plane $x_1/L_{pp} = 0.0175$ obtained with the 14 turbulence models tested. (a) SA and SKL$-V_1/V_\infty$.(b) SA and SKL$-(k \times 10^3)/V_\infty^2$.(c) MT and AKN$-V_1/V_\infty$(d) MT and AKN $-(k \times 10^3)/V_\infty^2$. (e) W88 and W98 $-V_1/V_\infty$. (f) W88 and W98 $-(k \times 10^3)/V_\infty^2$. (g) SST94 and SST03 $-V_1/V_\infty$. (h) SST94 and SST03 $-(k \times 10^3)/V_\infty^2$.

experimental data. Although the assessment of the modelling error based on Fig. 10 is purely qualitative, it is clear that the prediction of the flow field at the propeller plane is strongly dependent on the turbulence model. In general, the three models with the poorest resemblance to the experimental data are the SA, MT and AKN. On the other hand, the best qualitative agreement between experiments and simulations is obtained for the W98, EARSM[1], EARSM[2] and EARSM[3] models. From the remaining 7 models, the SST94 and SST03 show a better match with experiments than the remaining five models (SKL, W88, KSKL, BSL and TNT). However, it is important to point out that the models that exhibit the "hook-shape" of the V_1 isolines (originated by the bilge vortex) most similar to the experiments are also those that lead to the largest differences to the experiments (lowest values of V_1) below the bilge vortex region. Therefore, the assessment of the global performance of the different turbulence models becomes troublesome.

The quantitative assessment of the modelling error is illustrated in Fig. 11 for the MT and EARSM[1] models, which from the qualitative point of view correspond to one of the worst and one of the best turbulence models for the prediction of the flow field at the propeller plane. The results of Fig. 11a and b show that E_k is significantly smaller for the EARSM[1] simulation than for the MT results. However, for the

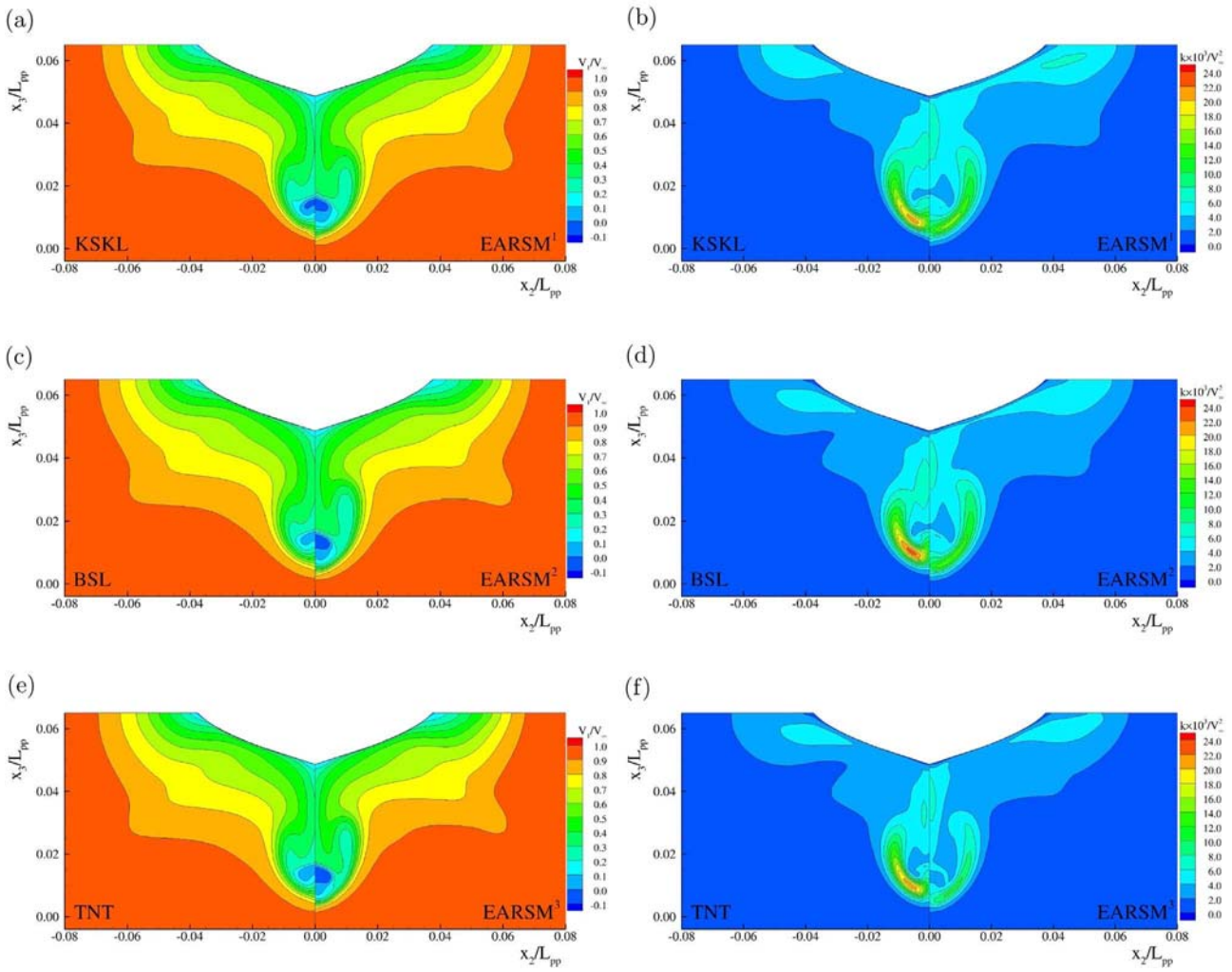

Fig. 10. (*continued*) (a) KSKL and EARSM[1] $-V_1/V_\infty$. (b) KSKL and EARSM[1] $-(k \times 10^3)/V_\infty^2$. (c) BSL and EARSM[2] $-V_1/V_\infty$. (d) BSL and EARSM[2] $-(k \times 10^3)/V_\infty^2$. (e) TNT and EARSM[3] $-V_1/V_\infty$. (f) TNT and EARSM[3] $-(k \times 10^3)/V_\infty^2$.

V_1 field the comparison errors are significantly smaller for the EARSM[1] data in the "hook shape" region, but there are values of E_{V_1} that reach 30% of V_∞ below the bilge vortex at the symmetry plane. The plots 11c–f of Fig. 11 present the minimum and maximum absolute values of the estimated modelling errors δ_{V_1} and δ_k. The white regions of the plots correspond to the estimated intervals that contain zero. The performance of the EARSM[1] model is clearly better than that obtained for the MT model, but for the present level of grid refinement, U_{val} at the regions with the largest gradients of V_1 and k is still significant. For example, in the EARSM[1] solution at $x_2 = 0$ and $x_3 = 0.01L_{pp}$, E_{V_1} reaches 35% of V_∞ and U_{val} 20% of V_∞. Nonetheless, the plots show that it is possible to identify the sign of the modelling error of V_1 for most of the propeller plane (Fig. 12).

An overall evaluation of the performance of the turbulence models in the prediction of the flow field at the propeller plane is achieved with the multivariate metric r/r_{ref} described in Section 3.5. We have calculated r/r_{ref} for the stream-wise V_1, transverse V_2 and vertical V_3 velocity components and turbulence kinetic energy k using different sets of experimental data[16]: wind tunnel (WT) (Lee et al., 2003); wind tunnel with the corrections (WT-C) suggested in Larsson et al. (2013) and towing tank (TT) (Kim et al., 2001). The data suggest the following remarks:

- For V_1 and V_2, there is a much better agreement of all the simulations with the towing tank data than with the wind tunnel results with or without corrections. For the vertical component V_3, the agreement with the TT data becomes much worse, most likely due to the effect of the free-surface;
- There is a slight decrease of the values of r/r_{ref} with the simple correction for blockage effects WT-C when compared to the values produced without it WT. However, the differences between WT and WT-C are much smaller than those obtained between the WT and TT data. Such result suggests that a rigorous comparison to the WT data should be performed including the wind tunnel walls in the simulations;
- The values of r/r_{ref} for the wind tunnel data are in general larger for V_1 than for k. However, this is a consequence of the U_{val} values that weight the metric r. Validation uncertainty is larger for k than for V_1;
- None of the turbulence models makes an overall prediction of the flow field within the level of the validation uncertainty. Nonetheless, the global trends obtained from the values of r/r_{ref} are similar to those discussed above for the qualitative performance of the turbulence models in the prediction of the flow field at the propeller plane. However, even with the limitations discussed above, in this case it is a quantitative assessment.

[16] k is only available for the wind tunnel tests.

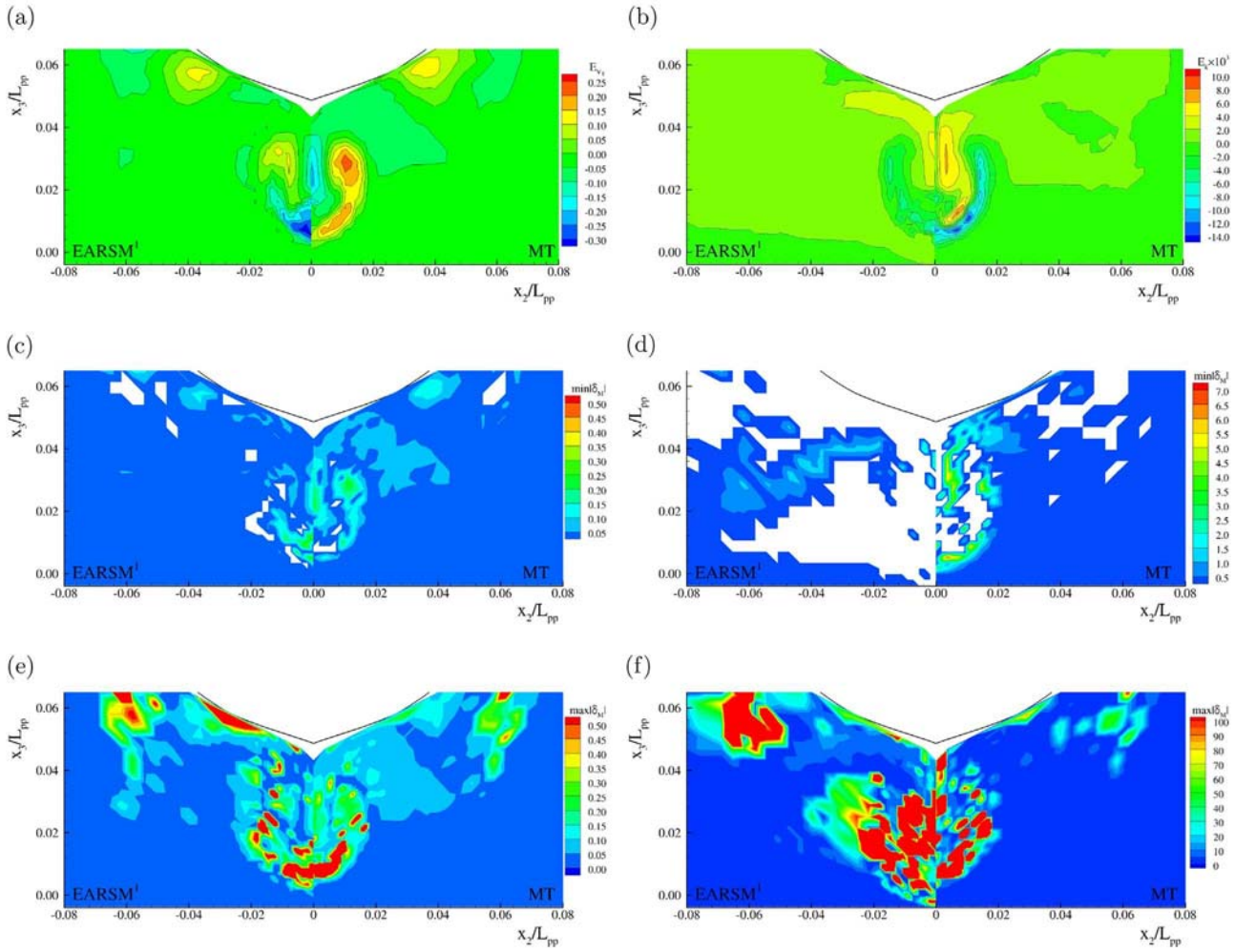

Fig. 11. Comparison error, E_ϕ, and maximum and minimum estimates of the modelling error, $|\delta_\phi|$, for the stream-wise velocity, V_1, and turbulence kinetic energy, k, fields at the propeller plane, $x_1/L_{pp} = 0.0175$. Results obtained for the MT and EARSM[1] models. Comparison error calculated with the measurements of Lee et al. (2003) (wind tunnel). (a) E_{ν_1/V_∞}. (b) $E_{k/V_\infty^2} \times 10^3$. (c) $\min|\delta_{V_1/V_\infty}|$. (d) $\min|\delta_{k/V_\infty^2}| \times 10^3$. (e) $\max|\delta_{V_1/V_\infty}|$. (f) $\min|\delta_M(k/V_\infty^2)| \times 10^3$

4.3. Scale-effects

The selected flow quantities for the illustration of the simulation of scale-effects are the form-factor $1+K$ and the wake-fraction coefficient W.

The form-factor is used to extrapolate viscous resistance coefficients from model to full-scale Reynolds numbers and is defined by

$$1 + K = \frac{C_T}{C_{F_0}}, \tag{31}$$

where C_{F_0} is the friction resistance coefficient obtained from the ITTC friction line (8th International Towing Tank Conference, 1957) ($C_{F_0} = 0.075/(\log_{10}(Re) - 2.0)^2$). In the standard ITTC extrapolation procedure, K is assumed to be independent of the Reynolds number. Naturally, the numerical uncertainty of the form-factor is given by $U_K = U_{C_T}/C_{F_0}$.

The wake-fraction W quantifies the stream-wise velocity deficit at the propeller disk and is defined by

$$W = 1 - \frac{\overline{V_1}}{V_\infty}, \tag{32}$$

where $\overline{V_1}$ is the average value of V_1 at the propeller disk.

Fig. 13 presents the values of $1+K$ and their respective uncertainties for the four turbulence models tested at model and full-scale Reynolds numbers. All turbulence models lead to a larger form-factor at full-scale than at model-scale. The largest increase of $1+K$ between model and full-scale is obtained for the SA model (7.62%) and the smallest for the KSKL model (3.47%). The SST94 and EARSM[3] model lead to an increase of the form-factors at full-scale of, respectively, 5.45% and 4.45%. The uncertainties U_{1+K} at model and full-scale varied between 7.54×10^{-3} and 5.18×10^{-2}, and only the results obtained with the SA and SST94 models guarantee an increase of $1+K$ from model to full-scale Reynolds number (no overlap in the error bars of Fig. 13). Nonetheless, the results of these simulations suggest that the usual hypothesis of assuming $1+K$ independent of the Reynolds number is, at least, questionable (VIRTUE – The Virtual Tank Utility in Europe, 2007a).

Table 4 presents the values of W and U_W at model and full-scale Reynolds numbers for the four turbulence models tested. W is based on the stream-wise velocity deficit at the propeller disk that is presented in Fig. 14 for the model and full-scale Reynolds numbers simulations performed with the EARSM[3] turbulence model. Naturally, the values of W at full-scale are significantly smaller than those obtained at model-scale. However, the predicted values of W depend on the selected turbulence model. The range of values of W obtained at model-scale corresponds to 24% of the average value of W of the four turbulence models, whereas at full-scale this range reduces to 10% of the average W of the four models. The ratio between the values of W at full and model-scale is 0.556 ± 0.016 for SA; 0.514 ± 0.008 for SST94; 0.484 ± 0.016 for EARSM[3] and 0.505 ± 0.022 for KSKL. Therefore, we

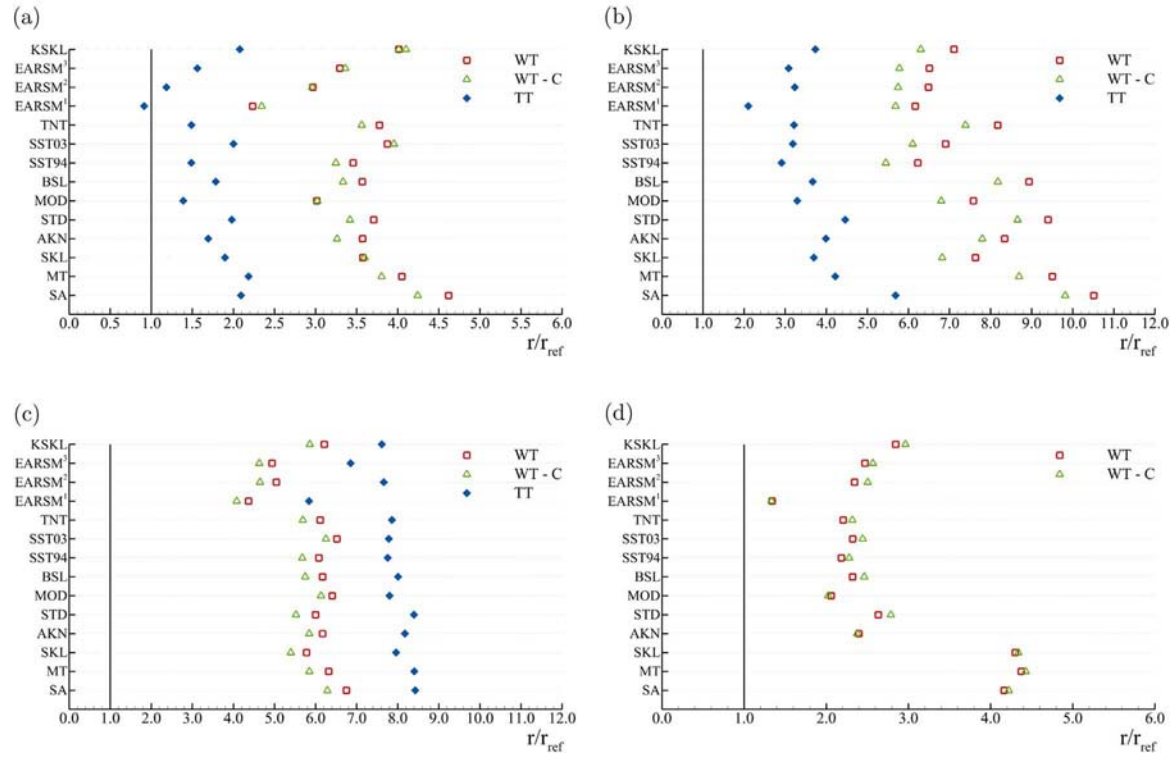

Fig. 12. Normalized multivariate metric r/r_{ref}, for the stream-wise V_1, transverse V_2 and vertical V_3 velocity components and turbulence kinetic energy k fields at the propeller plane $x_1/L_{pp} = 0.0175$. Three sets of experimental data tested: wind tunnel (WT) (Lee et al., 2003); wind tunnel with the corrections (WT-C) suggested in Larsson et al. (2013) and towing tank (TT) (Kim et al., 2001). (a) $r(V_1)/r_{ref}$. (b) $r(V_2)/r_{ref}$. (c) $r(V_3)/r_{ref}$. (d) $r(k)/r_{ref}$.

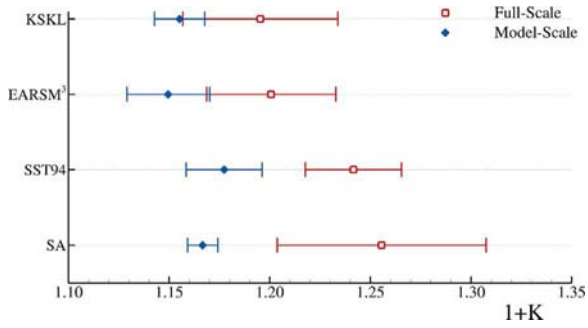

Fig. 13. Form-factor, $1+K$, and respective numerical uncertainty, U_{1+K}, obtained in the finest grid g_1 of the simulations at model $Re = 4.6 \times 10^6$ and full-scale $Re = 2.03 \times 10^9$ Reynolds numbers.

Table 4
Wake-fraction, W, and respective numerical uncertainty U_W obtained at model and full-scale Reynolds numbers in grid g_1 using the SA, KSKL, SST94 and EARSM^3 turbulence models.

Model	Re	W	U_w (%)
SA	4.60×10^6	0.437	2.00
	2.03×10^9	0.243	0.88
SST94	4.60×10^6	0.488	0.48
	2.03×10^9	0.251	1.05
EARSM^3	4.60×10^6	0.557	0.52
	2.03×10^9	0.270	2.97
KSKL	4.60×10^6	0.489	1.17
	2.03×10^9	0.247	3.20

obtain non-overlapping intervals of the ratio of W for the SA, SST94 and EARSM^3 models. The KSKL model leads to the largest uncertainty and so the interval obtained for this turbulence model overlaps the

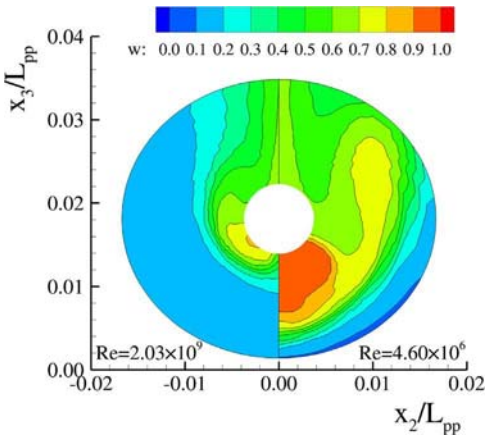

Fig. 14. Stream-wise velocity deficit at the propeller plane $x_1/L_{pp} = 0.0175$ for the EARSM^3 turbulence model at model and full-scale Reynolds number. Plotted region is $0.2R \leq r \leq 1.1R$, where R is the propeller radius.

SST94 and EARSM^3 solutions. Unfortunately, the evaluation of the quality of such predictions will require experimental data for full-scale Reynolds number (with matching conditions between experiments and simulations).

5. Conclusions

This paper presents the quantification of numerical and modelling errors for the simulation of the flow around the KVLCC2 tanker at model and full-scale Reynolds numbers. Fourteen RANS turbulence models are tested for model-scale Reynolds number ($Re = 4.60 \times 10^6$), including eleven eddy-viscosity models and three Explicit Algebraic Reynolds-Stress models. The Validation exercise is performed at model-scale for the resistance coefficient and the flow field (mean

velocity and turbulence kinetic energy) at the propeller plane. On the other hand, the wake-fraction and form-factor are the quantities selected to illustrate the simulation of scale-effects. Numerical uncertainties are estimated for all simulations performed with grid refinement studies, and modelling errors are evaluated using the ASME V&V20 procedures (The American Society of Mechanical Engineers, 2009, 2016) and experimental data available in the literature, which was obtained from wind tunnel and towing tank experiments. At full-scale Reynolds number ($Re = 2.03 \times 10^9$), only three isotropic eddy-viscosity models and one EARSM were tested. In the absence of experimental data, the discussion focused on the prediction of scale-effects.

All calculations were performed without wall-functions, and the effect of the free-surface is neglected. Blockage effects of the wind tunnel walls were not taken into account in the flow simulations and so none of the experiments available in the literature match exactly the simulation conditions. Furthermore, parameter/input uncertainties were assumed to be zero and experimental uncertainties were set equal to the values reported in the literature, which in some cases seem to be too optimistic (uncertainty is smaller than the asymmetry of the data). Nonetheless, a significant effort was made to reduce numerical uncertainties to acceptable levels using grids up to 21.0×10^6 cells with second-order schemes applied to the convective terms of the momentum equations, iterative convergence criteria that require maximum normalized residuals of all transport equations below 10^{-8} and (14 digits) double precision (model and full-scale).

The results obtained at model-scale Reynolds number suggest the following conclusions:

- As expected, the modelling error of the RANS equations in the simulation of the flow around the KVLCC2 tanker is strongly dependent on the selected turbulence model;
- For the same level of grid refinement, numerical uncertainties are dependent on the selected turbulence model. For the present level of grid refinement (finest grid with 20.1×10^6 cells), the estimated numerical uncertainties of the resistance coefficient are between 1% and 2% for most models tested, but one of the EARSM models leads to 6% uncertainty in C_T due to the existence of significant amount of scatter in the data. On the other hand, 40% of the locations of the propeller plane with available experimental data do not show monotonic convergence of the mean velocity components and turbulence kinetic energy for the grids with more than 4.9×10^6 cells. Therefore, the estimation of numerical uncertainties based on power series expansions is most likely too conservative;
- The turbulence models that lead to the smallest modelling errors in the resistance coefficient are not the same as those that lead to the smallest modelling errors in the prediction of the flow field at the propeller plane. For example, the one-equation model that leads to the smallest modelling error for the resistance coefficient exhibits one of the largest modelling errors for the flow field at the propeller plane. Similarly, the EARSM models that lead to the smallest modelling errors for the flow field at the propeller plane are among those that exhibit the largest modelling errors for C_T;
- The multivariate metric that quantifies the modelling error for multiple set points provides a good way to quantitatively compare the performance of different turbulence models. Furthermore, it also enhances the mismatches between experimental and simulation conditions. In the present exercise, with the exception of the vertical velocity component, there is a much better agreement between all simulations and the towing tank data than with the wind tunnel results (with or without blockage corrections).

The full-scale simulations demonstrated the numerical robustness of the implementation of the selected turbulence models. With the present level of numerical uncertainty, it is possible to confirm that simulations show a form-factor dependent on the Reynolds number, which contradicts the classical methods for extrapolation of viscous resistance coefficients. The discrepancies between the flow fields obtained at the propeller plane with different turbulence models tend to decrease with the increase of the Reynolds number. However, the reduction of the wake-fraction with the increase of the Reynolds number is clearly dependent on the selected turbulence model.

Although there are still some shortcomings in the Validation and Verification exercises reported in this paper, it is clear that the quantification of modelling errors must be pursued to improve the predictive capabilities of CFD models. This effort requires the knowledge of numerical and experimental uncertainties and so it would be desirable to have such values always reported.

Acknowledgements

The authors are very grateful to MARIN for the use of their computational resources, and to Dr. Suak-Ho Van from KRISO for sending his experimental measurements.

References

8th International Towing Tank Conference, 1957. Madrid, Spain.
Abbas, N., Schevchuk, I., Kornev, N., 2013. Development and validation of a hybrid RANS-LES method for ship hydromechanics applications. In: Proceedings of the 16th Numerical Towing Tank Symposium (NuTTS'13).
Abdel-Maksoud, M., Hellwig, K., Menter, F.R., 2000. Calculation of the turbulent flow around a model and full scale VLCC ship hull. In: Gothenburg 2000 – a Workshop on Numerical Ship Hydrodynamics.
Abe, K., Kondoh, T., Nagano, Y., 1994. A new turbulence model for predicting fluid flow and heat transfer in separating and reattaching flows – 1. Flow field calculations. Int. J. Heat. Mass Transf. 37 (1), 139–151.
Beddhu, M., Pankajakshan, R., Jiang, M.Y., Taylor, L.K., Remotigue, M.G., Briley, W.R., Whitfield, D.L., 2000. Computation and evaluation of CFD results for practical ship hull forms. In: Gothenburg 2000 – a Workshop on Numerical Ship Hydrodynamics.
Chou, S.K., Chau, S.W., Chen, W.C., Hsin, J.Y., 2000. Computations of ship flow around commercial hull form with free surface or propeller effect. In: Gothenburg 2000 – a Workshop on Numerical Ship Hydrodynamics.
Demirel, Y., Khorasanchi, M., Turan, O., Incecik, A., Schultz, M., 2014. A CFD model for the frictional resistance prediction of antifouling coatings. Ocean Eng. 89, 21–31.
Deng, G.B., Visonneau, M., 2000. Comparison of explicit algebraic stress models and second-order turbulence closures for steady flows around the KVLCC2 ship at model and full scales. In: Gothenburg 2000 – a Workshop on Numerical Ship Hydrodynamics.
Dol, H.S., Kok, J.C., Oskam, B., 2002. Turbulence modelling for leading-edge vortex flows. In: Proceedings of the 40th Aerospace Sciences Meeting and and Exhibit, American Institute of Aeronautics and Astronautics (AIAA).
Eça, L., Hoekstra, M., 2004. Eddy viscosity transport equations and their relation to the $k-\epsilon$ model. J. Fluids Eng. 126 (6), 900–910.
Eça, L., Hoekstra, M., 2009a. On the numerical accuracy of the prediction of resistance coefficients in ship stern flow calculations. J. Mar. Sci. Technol. 14 (1), 2–18.
Eça, L., Hoekstra, M., 2009b. Evaluation of numerical error estimation based on grid refinement studies with the method of the manufactured solutions. Comput. Fluids 38, 1580–1591.
Eça, L., Hoekstra, M., 2014. A procedure for the estimation of the numerical uncertainty of CFD calculations based on grid refinement studies. J. Comput. Phys. 262, 104–130.
Eça, L., Saraiva, G., Vaz, G., Abreu, H., 2015. The pros and cons of wall functions. In: Proceedings of the 34th International Conference on Ocean. Offshore and Arctic Engineering (OMAE2015).
Girimaji, S.S., 2005. Partially-averaged Navier-Stokes model for turbulence: a Reynolds-averaged navier-stokes to direct numerical simulation bridging method. J. Appl. Mech. 73 (3), 413–421.
Guo, B., Deng, G., Steen, S., 2013. Verification and validation of numerical calculation of ship resistance and flow field of a large tanker. Ships Offshore Struct. 8 (1), 3–14.
Guo, B., Steen, S., 2010. Computational study on ship resistance and flow field of KVLCC2. In: Gothenburg 2010 – a Workshop on Numerical Ship Hydrodynamics.
Hellsten, A., 2005. New advanced $k-\omega$ turbulence model for high-lift aerodynamics. Am. Inst. Aeronaut. Astronaut. (AIAA) J. 43 (9), 1857–2869.
Hills, R.G., 2006. Model validation: model parameter and measurement uncertainty. Am. Soc. Mech. Eng. (ASME) J. Heat. Transf. 128, 339–351.
Hoekstra, M., Eça, L., Windt, J., Raven, H., 2000. Viscous flow calculations for KVLCC2 and KCS models using PARNASSOS code. In: Gothenburg 2000 – a Workshop on Numerical Ship Hydrodynamics.
Khor, Y., Xiao, Q., 2011. CFD simulations of the effects of fouling and antifouling. Ocean Eng. 38 (10), 1065–1079.
Kim, W.J., Van, S.H., Kim, D.H., 2001. Measurement of flows around modern commercial ship models. Exp. Fluids 31 (5), 567–578.
Kim, J., Park, I.-R., Kim, K.-S., Van, S.-H., 2010. Feasibility study on numerical towing tank application to predictions of resistance and self-propulsion performances for a

ship. In: Gothenburg 2010 – a Workshop on Numerical Ship Hydrodynamics.
Kim, S.-E., 2000. Reynolds stress transport modeling of turbulent shear flow past a modern VLCC hull form. In: Gothenburg 2000 – a Workshop on Numerical Ship Hydrodynamics.
Kim, W.J., Van, S.H., 2000. Comparison of turbulent flow around two modern VLCC hull forms. In: Gothenburg 2000 – a Workshop on Numerical Ship Hydrodynamics.
Kok, J.C., 2000. Resolving the dependence on freestream values for the $k-\omega$ turbulence model. Am. Inst. Aeronaut. Astronaut. (AIAA) J. 38 (7), 1292–1295.
Larsson, L., Stern, F., Visonneau, M. (Eds.), 2013. Numerical Ship Hydrodynamics: An Assessment of the Gothenburg 2010 Workshop. Springer, Netherlands.
Launder, B.E., Sharma, B.I., 1974. Application of the energy-dissipation model of turbulence to the calculation of flow near a spinning disc. Lett. Heat. Mass Transf. 1 (2), 131–137.
Lee, S.J., Kim, H.R., Kim, W.J., Van, S.H., 2003. Wind tunnel test on flow characteristics of the KRISO 3,600 TEU containership and 300 K VLCC double-deck ship models. J. Ship Res. 47 (1), 24–38.
Martio, J., Caja, A.S., Sipilä, T., Saisto, I., Siikonen, T., 2010. Simulation of free-surface flow using code FINFLO for KVLCC2 and KCS cases. In: Gothenburg 2010 – a Workshop on Numerical Ship Hydrodynamics.
Menter, F.R., 1994. Two equation eddy-viscosity turbulence models for engineering application. Am. Inst. Aeronaut. Astronaut. (AIAA) J. 32 (8), 1598–1605.
Menter, F.R., 1997. Eddy viscosity transport equations and their relation to the $k-\epsilon$ model. J. Fluids Eng. 119 (4), 876–884.
Menter, F.R., 2003. Ten years of industrial experience with the SST turbulence model. In: Turbulence, Heat and Mass Transfer. vol. 4, pp. 625–632.
Menter, F.R., Egorov, Y., Rusch, D., 2006. Steady and unsteady flow modelling using $k-\sqrt{k}L$ model. In: Proceedings of the 5th International Symposium on Turbulence, Heat and Mass Transfer.
National Maritime Research Institute (NMRI), 2015. Tokyo 2015 A Workshop on CFD in Ship Hydrodynamics.
Nishikawa, T., Yamade, Y., Sakuma, M., Kato, C., 2012. Application of fully-resolved large eddy simulation to KVLCC2. J. Jpn. Soc. Nav. Archit. Ocean Eng. 16, 1–9.
Nishikawa, T., Yamade, Y., Sakuma, M., Kato, C., 2013. Fully resolved large simulation as an alternative to towing tank resistance test – 32 Billion cells computation on K computer. In: Proceedings of the 16th Numerical Towing Tank Symposium (NuTTS'13).
Oberkampf, W.L., Roy, C.J., 2010. Standard for Verification and Validation in Computational Fluid Dynamics and Heat Transfer – ASME V & V 20-2009. Cambridge University Press.
Pereira, F.S., Vaz, G., Eça, L., 2015a. On the numerical requirements of RANS and hybrid turbulence models. In: Proceedings of the VI International Conference on Computational Methods in Marine Engineering (MARINE2015).
Pereira, F.S., Vaz, G., Eça, L., 2015b. An assessment of scale-resolving simulation models for the flow around a circular cylinder. In: Turbulence, Heat and Mass Transfer 8.
Raven, H.C., 2016. Private Communication.
ReFRESCO, 2016. ⟨www.refresco.org⟩.
Rhee, S.H., Hino, T., 2000. Unstructured grid flow solver for practical ship hulls. In: Gothenburg 2000 – a Workshop on Numerical Ship Hydrodynamics.
Roache, P.J., 1998. Verification and Validation in Computational Science and Engineering. Hermosa Albuquerque.
Roache, P.J., 2009. Fundamentals of Verification and Validation. Hermosa Albuquerque.
Rumsey, C.L., Reif, B.A.P., Gatski, T.B., 2006. Arbitrary steady-state solution with the K-Epsilon model. Am. Inst. Aeronaut. Astronaut. (AIAA) J. 44 (7), 1586–1592.
Schneider, M., 2010. RANS simulation of the flow around the KVLCC2 tanker using the FreSCO$^+$ code. In: Gothenburg 2010 – a Workshop on Numerical Ship Hydrodynamics.
Spalart, P.R., Allmaras, S.R., 1992. A one-equation turbulence model for aerodynamic flows. In: American Institute of Aeronautics and Aerospace 30th Aerospace Sciences Meeting and Exhibit.
Spalart, P.R., Jou, W.-H., Stretlets, M., Allmaras, S., 1997. Comments on the feasibility of LES for wings and on the hybrid RANS/LES approach. In: Proceedings of the First Air Force Office of Scientific Research International Conference on DNS/LES – Advances in DNS/LES.
Svennberg, S.U., 2000. A test of turbulence models for steady flows around ships. In: Gothenburg 2000 – a Workshop on Numerical Ship Hydrodynamics.
The American Society of Mechanical Engineers (ASME), 2009. Standard for verification and validation in computational fluid dynamics and heat transfer – ASME V & V 20-2009. The American Society of Mechanical Engineers.
The American Society of Mechanical Engineers (ASME), 2016. Multivariate Metrics – Supplement 1 of ASME V & V 20-2009. The American Society of Mechanical Engineers.
Toxopeus, S.L., Simonsen, C.D., Guilmineau, E., Visonneau, M., Xing, T., Stern, F., 2013. Investigation of water depth and basin wall effects on KVLCC2 in manoeuvering motion using viscous-flow calculations. J. Mar. Sci. Technol. 18 (4), 471–496.
Toxopeus, S., 2011. Viscous-flow calculations for KVLCC2. In: Deep and Shallow Water. In IV International Conference on Computational Methods in Marine Engineering (MARINE2011).
Toxopeus, S.L., Tormalm, M., Petterson, K., Johansson, M., Fureby, C., 2014. A computational study of the flow around the KVLCC2 model hull at straight ahead conditions and at drift. In: Proceedings of the 30th Symposium on Naval Hydrodynamics.
VIRTUE – The Virtual Tank Utility in Europe, 2007a. Results for the workshop on resistance prediction. In: Work Package 1: The Virtual Towing Tank. Project 516201, TIP5-CT-2005-516201.
VIRTUE – The Virtual Tank Utility in Europe, 2007b. Workshop on resistance prediction. In: Work Package 1: The Virtual Towing Tank. Project 516201, TIP5-CT-2005-516201.
Wallin, S., Johansson, A.V., 2000. An explicit algebraic reynolds stress model for incompressible and compressible turbulent flows. J. Fluid Mech. 403, 89–132.
Wilcox, D.C., 1988. Reassessment of the scale-determining equation for advanced turbulence models. Am. Inst. Aeronaut. Astronaut. (AIAA) J. 26 (11), 1299–1310.
Wilcox, D.C., 1998. Turbulence Modelling for CFD first ed.. DCW Industries.
Xing, T., Stern, F., 2010. Factors of safety for richardson extrapolation. J. Fluids Eng. 132 (6), (061403-061403-13).
Xing, T., Carrica, P., Stern, F., 2010. Large-scale RANS and DDES computations of KVLCC2 at drift angle 0 degree. In: Gothenburg 2010 - A Workshop on Numerical Ship Hydrodynamics.
Yu, H., Feng, X.-M., Wu, Q., Wang, J.-B., Cai, R.-Q., 2010. Prediction of ship resistance and propulsion performance using multi-block structured grids. In: Gothenburg 2010 – a Workshop on Numerical Ship Hydrodynamics.